REPORT DOCUMENTATION PAGE

Form Approved
OMB No. 0704-0188

PLEASE DO NOT RETURN YOUR FORM TO THE ABOVE ORGANIZATION.

1. REPORT DATE *(DD-MM-YYYY)*	2. REPORT TYPE	3. DATES COVERED *(From - To)*
01-06-09	FINAL REPORT	1 APR 06 - 30 NOV 07

4. TITLE AND SUBTITLE

Directionally Solidified Eutectic Ceramics For Multifunctional Aerospace Applications

5a. CONTRACT NUMBER

5b. GRANT NUMBER

FA9550-06-1-0259

5c. PROGRAM ELEMENT NUMBER

6. AUTHOR(S)

Sayir, Ali

5d. PROJECT NUMBER

5e. TASK NUMBER

5f. WORK UNIT NUMBER

7. PERFORMING ORGANIZATION NAME(S) AND ADDRESS(ES)

Case Western Reserve University
10900 Euclid Avenue
Cleveland, OH 44106

8. PERFORMING ORGANIZATION REPORT NUMBER

9. SPONSORING/MONITORING AGENCY NAME(S) AND ADDRESS(ES)

AFOSR
875 N. Randolph St.
Suite 325
Arlington, VA 22203

10. SPONSOR/MONITOR'S ACRONYM(S)

AFOSR

11. SPONSOR/MONITOR'S REPORT NUMBER(S)

AFRL-OSR-VA-TR-2012-0405

12. DISTRIBUTION/AVAILABILITY STATEMENT

A

13. SUPPLEMENTARY NOTES

14. ABSTRACT

This project addresses the several challenges associated with incorporating structural ceramics in future aerospace applications: (1) the challenges associated with ceramics are improving strength, toughness and creep resistance retaining the mechanical properties at elevated temperatures and (2) to elucidate and demonstrate the multifunctional potential of the polyphase eutectic structures.

15. SUBJECT TERMS

16. SECURITY CLASSIFICATION OF:			17. LIMITATION OF ABSTRACT	18. NUMBER OF PAGES	19a. NAME OF RESPONSIBLE PERSON
a. REPORT	b. ABSTRACT	c. THIS PAGE		33	Dr. Joan Fuller
					19b. TELEPHONE NUMBER *(Include area code)* 703-696-8457

Reset

Standard Form 298 (Rev. 8/98)
Prescribed by ANSI Std. Z39.18

Progress Report for 2006

For the Grant

Directionally Solidified Eutectic Ceramics For Multifunctional Aerospace Applications

FA9550-06-1-0259

Submitted to

Dr. Joan Fuller

Air Force Office of Scientific Research

By

Dr. A. Sayir

CASE WESTERN RESERVE UNIVERSTY

SUMMARY

This project addresses the several challenges associated with incorporating structural ceramics in future aerospace applications: (1) the challenges associated with ceramics are improving strength, toughness and creep resistance retaining the mechanical properties at elevated temperatures and (2) to elucidate and demonstrate the multifunctional potential of the polyphase eutectic structures.
We pursued these objectives simultaneously in order for structural ceramics to be incorporated into aerospace applications. We report progress on three different areas:

1. The mechanical properties of polyphase Al_2TiO_5 - Al_2O_3 system eutectic, which showed superior mechanical properties than the either constituent alone due to the strong constraining effects provided by the coherent interfaces and microstructure.

2. The preliminary results on ultra high temperature eutectic materials development through a new initiative entitled Boride Eutectic Project. These results first time organize and populate materials property databases, and utilize an iterative feedback routine to constantly improve the design process of the boride eutectics LaB_6-MeB_2 (Me = Zr, Hf, Ti, Eu) are currently being developed by Dr. Filipov and Dr. V. Paderno at the Ukrainian Academy of Sciences and modeled by Dr. Kartuzov.

3. Directionally solidified eutectic ceramic process yields microstructures that have eutectic architecture of a continuous reinforcing phase within a higher volume phase or matrix, can be described as a naturally occurring *in-situ* composite. The physical properties of polyphase eutectic structure offer unique potential for multifunctional material development. We have previously reported on the progress of hydrogen membrane and thus we will include in this report the significant progress that we achieved on this topic since it will be reported separately by Drs. Marie-Helen Berger /Ecole des Mines des Paris and Pascal Berger / Laboratory Pierre Sue-France. The publication list provided at the end of the report will give good insight about the solid progress on high temperature proton conducting membranes. We reported also preliminary results on a new class thermoelectric materials for load bearing and waste heat recovery applications which are truly multifunctional materials. This work is ongoing and detailed information will be provided next year.

For the duration of first year, we published 27 journal articles. The list of our publications provided in the Appendix. The quality and number of publications demonstrates a tremendous progress for the multifunctional material development for aeronautic and aerospace structures. We organized an international conference on December 2006 on the directionally solidified eutectic ceramic in Kyoto, Japan.

I) Progress Report on Directional Solidification of Al_2TiO_5 - Al_2O_3 System and and Characterization of Intergrowth Formation of $Al_6Ti_2O_{13}$ and Al_2TiO_5 Phases

Directionally solidified eutectic (DSE) ceramics have the potential as structural components at elevated temperatures in applications ranging from aerospace to energy harvesting. The strong interphase bonding and large aspect ratio of the constituent phases characteristic of the directionally solidified eutectic ceramics are in large part responsible for their superior creep resistance and high temperature microstructural stability [1]. The interfaces between the two phases of eutectic structure typically adopt low-energy orientation relationships during the directional solidification process, this provides strong bonding [5, 6, 7] and prevents significant interface debonding. The degree of microstructural anisotropy of DSE ceramics, although a necessary condition in promoting improvements in high temperature mechanical properties, is insufficient to achieve higher toughness. The eutectic lamellae have little effect in diverting the path of the fracture crack. It is however conceivable that through incorporation of controlled amounts of primary phase, the fracture energy of a brittle eutectic matrix could be increased. The protruding plates or rods are expected to promote crack deflection at the interfaces between eutectic and primary phase in carefully engineered systems. To examine these postulations, Al_2TiO_5 - Al_2O_3 system was selected for directional solidification study. The range of structures that can be produced by off-eutectic solidification was examined to determine the increase in toughness that can be obtained by introducing a controlled amount of primary phase. Examination of the alumina rich part of the pseudo binary Al_2O_3 – TiO_2 phase diagram indicates a eutectic invariant point at 44 mole % of TiO_2, between Al_2O_3 and Al_2TiO_5 [8, 9, 10]. For lower titania content, the off eutectic composition is expected to solidify into primary alumina dendrites or plates embedded in an Al_2O_3 - Al_2TiO_5 eutectic matrix. The Al_2O_3 - Al_2TiO_5 eutectic structure is expect to consist of two interpenetrated single crystals of Al_2O_3 and Al_2TiO_5. The primary alumina phase would act as a high-stiffness reinforcing component to carry the load and provide strength. This work aims to utilize the anisotropy of the pseudobrookite structure of Al_2TiO_5 phase [11] and high thermal expansion mismatch between Al_2O_3 and Al_2TiO_5 phases to realize improved toughness. It is expected that controlled microcrack formation will be promoted along specific Al_2O_3 and Al_2TiO_5 interfaces or in one of the constituent phases [12, 13**]**. The length of the cracks would be restricted by the tortuosity of the primary phase and orientation changes of the Al_2O_3/Al_2TiO_5 interfaces in the eutectic structure. The microcracked matrix and weak interfaces would contribute to the toughness of the *in-situ* composite. The proposition of the weak interface between the constituent phases for the *in-situ* composite requires an in-depth understanding of the interface structure.

The selection of directional solidification approach implemented in present work as a processing method of Al_2O_3 - Al_2TiO_5 system had at least two advantages. First, the solidification approach is expected to facilitate the understanding of the toughening mechanisms in the Al_2O_3-Al_2TiO_5 eutectic system [14, 15]. As will be discussed extensively, the decohesion along the interfaces between alumina primary phase and eutectic matrix phase is also expected to occur locally and globally by the same mechanism and to increase the toughness. Finally, the Al_2TiO_5 is very difficult to sinter due to microcrack formation and as a result of this it has a very poor strength. Thus, there is an interest to improve the mechanical strength and toughness concurrently. The directional solidification approach offers opportunity to engineer structures that can have high strength and high toughness concurrently [14, 15]. In addition, the phase diagram of Al_2O_3-Al_2TiO_5 system [8, 9, 10] and the expected solidification reaction at the eutectic invariant point was attractive to produce desirable phase distribution and microstructures. This report presents characterization of the structure, morphology and distribution of phases and their solidification from the alumina rich side of the phase diagram. A systematic electron optic study was carried out to elucidate the new phase that has not been reported in previous phase diagrams and an outline of an alternative phase diagram has been proposed. The microstructural characterization presented in this report also aids for the understanding of the toughening concept of polyphase structures that promotes microcrack formation and debonding [14, 15]

Results are organized in two major sections. The first section presents the analyses of the phase distribution up to the micron-scale by the combination of WDX, SEM and XRD experiments. The second section is devoted to the nano-scale investigation of the structure and chemistry of the interfaces using TEM and STEM-EDX. In addition, cell parameters of the phases and crystal orientation relationships are presented from high resolution TEM investigation.

3-1 Composition and distribution of the phases

Eutectic composition (43.9 mol % TiO_2)

The solidification at the eutectic composition, AT44, produced a two phase lamellar structure, **Fig 1.** From the phase diagram, the expected phases are α-Al_3O_3 and β-Al_2TiO_5. However the corresponding x-ray diffraction spectrum shown in **Fig 2** contained no alumina peaks. The only diffraction peak that could possibly be originating from 020 reflection of β-Al_2TiO_5[1] phase, was located at 2θ=18.79° and marked as "$\triangle$". All the other peaks, marked as "∇", had a significant shift from the expected position of β-Al_2TiO_5 diffraction peaks. The quantitative WDX analysis, shown in **Figure 3,** demonstrated that the composition of the major phase, shown as darker phase in Fig. 1, was close to the nominal composition of $Al_6Ti_2O_{13}$ ($3Al_2O_3 \bullet 2TiO_2$). The composition of the brighter phase corresponded to that of the nominal composition of Al_2TiO_5 ($Al_2O_3 \bullet TiO_2$) phase. The phases were continuous in the growth direction as shown in **Fig. 1a**. In the plane normal to the growth direction, the minor phase of Al_2TiO_5 was discontinuous as shown in **Fig. 1b** and the lamellae were arranged in colonies of distinct orientations. Although colony boundaries were very small in comparison to other oxide eutectic structures [20], cracks were detected in the colony boundaries. The lamella width was approximately 2 μm for Al_2TiO_5 and 5μm for $Al_6Ti_2O_{13}$.

Off Eutectic Compositions (11 and 26.4 mol % TiO_2)

The XRD spectra of the materials solidified at the off-eutectic compositions, samples AT11 and AT26, showed a set of α-Al_2O_3 peaks marked as "•" in **Fig. 2.** The others peaks belonged to the set of peaks identified for the "eutectic" AT44 sample. From the sample AT11 only one weak peak could be unambiguously attributed to $Al_6Ti_2O_{13}$ phase. The examination of the SEM images, **Fig 4 and 5,** combined with WDX analyses showed that Al_2O_3 solidified into dendrites (dark phase) as primary phase for both AT11 and AT26 compositions. These primary dendrites were surrounded by a light grey phase containing Al, Ti, and O. The quantitative WDX analysis of this Al-Ti-O phase was carried out for the AT26 composition and the spatial distribution of elements is shown in **Fig. 6**. This experimentally measured composition is very close to that of the molar composition of $Al_6Ti_2O_{13}$ (= $3Al_2O_3 \bullet 2TiO_2$). The analysis was carried out at one-micrometer intervals over a length scale of 30 μm and had depth and lateral resolution of 2 μm. Uncertainty in concentration measurements for Al, Ti, O resulted in a total concentration of 101 wt%. The chemical variation in the length scale of the characterization was not significant within the experimental uncertainty. The inter-dendrite phase was not a two-phase eutectic. This was contrary to what was expected from the phase diagram for the off eutectic solidification. Similarly, a thin interdendritic region has been observed in the samples of the composition AT11 and due to small size of this region quantitatively analysis could not be accomplished using WDX. The TEM analysis shown below will describe that this phase indeed corresponds to $Al_6Ti_2O_{13}$ composition as in the AT26 sample. A third phase of approximately 1 μm in width could be detected along the alumina dendrites in sample AT26, as shown with arrows in Figure 5c as a bright phase. The small width of this phase prohibited any quantitative analysis by WDX and hence was analyzed with TEM. Neither the results relating to phase content nor the quantitative phase compositions determined from the specimens solidified at the off-eutectic composition does agree with the previously published phase diagrams [21]. Although solidification condition is by definition is not an equilibrium process, these findings have an important conjecture for the existing phase diagram that is worthy to emphasize.

The structure of the directionally solidified ceramic at the off-eutectic composition consisted of two spatially different microstructural regions, an outer rim region and central region. The outer rim region was around 50 μm in width for the AT11 and 150 μm for the AT26 compositions and contained closely packed Al_2O_3 dendrites (**Fig. 4c, 5a,b**) that were strongly tilted up to 45° with respect to the growth axis. The lateral dimensions of the outer dendrites were close to the width dimensions of the outer rims. The central regions of samples AT11 and AT26 exhibited well-developed dendrites that were well aligned with the growth axis. In the material solidified at the alumina rich side of the phase diagram, sample AT11 (11 mol % TiO_2), the length of the dendrites could reach 2 mm and widths of 20μm. Cracks were observed at the Al_2O_3 / $Al_6Ti_2O_{13}$ interface. Materials solidified at 26 mol % TiO_2 composition had significantly smaller dendrite lengths (up to 1 mm) but larger width, ~50 μm, in comparison to 11 mole % TiO_2 composition. The volume fraction of the Al_2O_3 dendrites was reduced, and they were highly

[1] In this work, indexations of directions and planes of β-Al_2TiO_5 crystal refer to orthorhombic system, with a c-face centred unit cell, space group Cmcm, a=3.593 Å, b=9.439 Å, c=9.647 Å , in accordance with notations used by Göbbels et al. [15], Mazerolles et al.[16], Norberg et al [17]. Morosin and Lynch [18] and JCPDF card 41-0258 describe the crystal using the equivalent space group Bbmm , a=9.439 Å, b=9.647 Å , c=3.593 Å.

interpenetrated by primary $Al_6Ti_2O_{13}$ phase. Relatively large cracks (up to 200μm) were found throughout the $Al_6Ti_2O_{13}$ phase.

3.2. Structure of the phases and interphases developed - Orientation Relationship between the phases

The structure and chemistry of heterophase interfaces in directionally solidified eutectic structures have a major impact on the mechanical performance of the systems. As pointed out above, the resolutions of techniques (SEM, WDX and XRD) were not sufficient to identify the nature of the bright interphase between Al_2O_3 and $Al_6Ti_2O_{13}$ for the off eutectic samples. In the same way, the interface structure between $Al_6Ti_2O_{13}$ and Al_2TiO_5 in eutectic samples could not be analysed. This section presents a nano-scale analysis of the phases and interfaces using STEM-EDX and high resolution TEM.

Interphase between α–Al_2O_3 and $Al_6Ti_2O_{13}$

Figure 7a) is a representative TEM micrograph of 26 mol % TiO_2 composition with the $Al_6Ti_2O_{13}$ matrix and a α–Al_2O_3 dendrite at the left and right sides of the micrograph, respectively. In addition, an interphase was observed between the two phases, as was described previously on the SEM image of **Fig 5c**. Qualitative variations of Al, Ti and O concentrations were investigated across the three-phase region (shown in the Fig. 7a as white line) using STEM-EDX profile technique. The interphase phase was richer in titanium than the nominal $Al_6Ti_2O_{13}$ composition as shown by Fig 7b. High resolution TEM images of this interphase in **Figure 8a** shows two orthogonal sets of planes with interplanar distances of ~4.7 Å and ~9.6 Å. These results indicated that the interphase corresponded to the Al_2TiO_5 phase as observed in [100] zone axis and characterized by (020) and (001) planes. TEM observations have been undertaken for 11 mol % TiO_2 composition and Fig. 9a presents a representative TEM image of an interdrendritic region and Fig. 9b a STEM-EDX qualitative profile across the interphase region. The constituent phases and HRTEM microstructural analysis results were analogous to those of AT26 and thus will not be repeated here.

Cell Parameters of $Al_6Ti_2O_{13}$

Figure 8b is a high-resolution image of $Al_6Ti_2O_{13}$ from location depicted in the left side of Fig 7 and taken in the same orientation of the TEM foil as Fig. 8a at the Al_2TiO_5 interphase. Figure 8c is a selected area diffraction (SAD) pattern of $Al_6Ti_2O_{13}$ for the same [100] zone axis. The vertical planes have inter-planar distance of ~4.7 Å which was similar to d_{020} of Al_2TiO_5. The reflection orthogonal to 020 corresponded to distance of 12.5 Å and was assigned to 001 of $Al_6Ti_2O_{13}$. The comparison of **Fig. 8 a** and **b** confirms the relationship $5d_{001,Al_2TiO_5} \approx 4d_{001,Al_6Ti_2O_{13}}$. **Figure 10a** is a lattice fringe image of a $Al_6Ti_2O_{13}$ – Al_2TiO_5 interface region and corresponding Fast Fourier Transformation (FFT) is presented in **Figure 10b**. Both phases are in [001] zone axis. **Figure 10b** exhibits 020 reflection (4.7 Å) of Al_2TiO_5 and $Al_6Ti_2O_{13}$, and 110 (3.36 Å) reflection of Al_2TiO_5 at 69°6 from 020 reflection. The reflection 110 of $Al_6Ti_2O_{13}$ is slightly closer to the center than the 110 of Al_2TiO_5 and angle between the 100 and 110 reciprocal directions for $Al_6Ti_2O_{13}$ is also smaller than for Al_2TiO_5. The inter-planar distance of the 110 from $Al_6Ti_2O_{13}$ as determined from Fig.10b is 3.4 Å. From the measurements of 020, 001 and 110 interplanar distances and angles the structure of $Al_6Ti_2O_{13}$ was assumed to be orthorhombic with the following cell parameters:

a = 3.65 Å , b = 9.4 Å , c = 12.5 Å within the resolution of measurement pertinent to SAD and FFT of TEM images.

Orientation Relationship

Figures 11 and 12 are HRTEM images of $Al_6Ti_2O_{13}$ / Al_2TiO_5 / Al_2O_3 interphase regions in off eutectic sample AT26. The thin foil was extracted from a cross section of the rod that was perpendicular to the solidification direction. The images were obtained with a tilt angle closed to 0º and $Al_6Ti_2O_{13}$ and Al_2TiO_5 were observed in [100] zone axis. In this configuration, [100] zone axis corresponds to growth axis of the aluminum titanate phases. The *a*-, *b*-, and *c*- axes of $Al_6Ti_2O_{13}$ and of Al_2TiO_5 were aligned systematically. $Al_6Ti_2O_{13}$ / Al_2TiO_5 interfaces were non planar, often wavy as in Fig 7 and did not correspond to dense planes of the structures. The identical orientation of the $Al_6Ti_2O_{13}$ and Al_2TiO_5 cells across the interface was favourable for a simple reconstruction at the boundary as shown in Fig 12. The interface was curved and was not observed edge on, but could consist of (010) nano-facets to accommodate the disorientation of the interface. The interface plane shown in Fig. 11 was tilted 15° from (010) planes. The (001) planes are continuous across the $Al_6Ti_2O_{13}$/Al_2TiO_5 interface except at the tip of the white arrows where (001) planes of Al_2TiO_5 terminate at the interface. The misfit between (001) planes of $Al_6Ti_2O_{13}$ and Al_2TiO_5 was accommodated through the discontinuation of (001) planes of Al_2TiO_5

without clear periodicity. The crystal orientation of Al_2O_3 varied from one dendrite to another with respect to the growth axis. In a given specimen when aluminum titanates were in [100] zone axis (growth axis), low index zone axis of alumina could not be found as shown Fig 11, whereas α-Al_2O_3 was observed in another location of foil in the [10-11] zone axis as shown in Fig 12. As a result, no simple orientation relationship and interfaces between Al_2TiO_5 and Al_2O_3 were ascertained in most of the cases. The interface characteristics of AT11 composition were similar to aforementioned results of AT26 and will not be repeated here.

In the eutectic sample, the *a*-, *b*-, and *c*- axes of $Al_6Ti_2O_{13}$ and of Al_2TiO_5 phases were aligned systematically and the growth axis was parallel to the [100] direction. The long axes of the lamellae were parallel to [010] direction. The $Al_6Ti_2O_{13}/Al_2TiO_5$ interfaces were built along (001) planes, as seen in **Fig 13**. This HRTEM image shows a super structure in the growth sequence of the (001) planes in the "$Al_6Ti_2O_{13}$" phase. The following section presents an analysis for the origin of this superstructure.

Intergrowth

The super structure in the growth sequence of the (001) planes revealed in the matrix phase of eutectic samples gives rise to periodic superlattice reflections in the [001]* reciprocal direction with a periodicity of ~7 nm. This superstructure was formed by the intergrowth of the Al_2TiO_5 and $Al_6Ti_2O_{13}$ phases. The periodicity of ~7 nm corresponded to a supercell made of one block of Al_2TiO_5 (9.6 Å) and five blocks of $Al_6Ti_2O_{13}$ (12.5 Å) which was refereed as "1:5". Locally, this periodicity could be broken by shorter sequences of intergrowth such as one block of Al_2TiO_5 and four blocks of $Al_6Ti_2O_{13}$ or "1:4". **Figure 13d)** exemplifies such an intergrowth between Al_2TiO_5 and $Al_6Ti_2O_{13}$ in AT44. The Al_2TiO_5 blocks were marked with diamonds, and the sequence is 1:5 - 1:4 - 1:5.

Lines of black contrast were observed inside the $Al_6Ti_2O_{13}$ phase in the off eutectic sample and micrograph representing this attribute is shown in **Figure 7a** (at the tip of the double arrows). The distribution of these defects was not periodic and their density was low. The high resolution image shown in **Figure 14** revealed that the contrast was associated with a perturbation in the stacking sequence in the [001] direction. A single plane with an interplanar distance of ~9 Å was inserted between the planes (001) of $Al_6Ti_2O_{13}$. This shows evidence of some degree of intergrowth between the Al_2TiO_5 and $Al_6Ti_2O_{13}$ phases in the off eutectic also.

3.5. Eutectoid Decomposition

Samples with composition of 11, 26 and 43.9 mol % TiO_2 were annealed to assess the stability of the $Al_6Ti_2O_{13}$ phase. Samples were heated for 10 min at 1400°C (immediate placement in the furnace which was at steady state temperature and immediate removal from the furnace to room temperature). For these short heat treatments, a white and large outer rim region formed around a dark core region. The decomposition of the $Al_6Ti_2O_{13}$ phase was observed after heat treatment for 5 hours at 1400°C and a representative micrograph of a heat treated sample is shown in **Figure 15** for the 26 mol % TiO_2 composition. This annealing treatment turned the specimens with 11, 26 and 43.9 mol % TiO_2 compositions to white colour in their whole section. The dimension of the phases formed by the eutectoid reaction was not large enough to allow chemical analysis by WDX. **Figure 16** represents the result of a heat treatment at 1500 °C for 10 hours for the 12, 26 and 43.9 mol % TiO_2 compositions. The WDX analysis showed that the three samples were composed of alumina (grey) and Al_2TiO_5 (white phase) after this heat treatment. The Al_2TiO_5 phase between the Al_2O_3 dendrites in 11 mol % TiO_2 composition was not any longer continuous, but composed of rounded grains. Sample with the 26 mol % TiO_2 composition contained precipitates of Al_2O_3 that were included in the Al_2TiO_5 phase. The Al_2TiO_5 phase in 43.9 mol % TiO_2 composition (eutectic point) had a lamellae structure prior annealing and was aligned along the growth direction. The high temperature annealing increased the width of the Al_2TiO_5 phase and frequency of contacts with other Al_2TiO_5 lamellae. Similarly, the precipitated Al_2O_3 phase build spherical grains and these were aligned in rows parallel to the Al_2TiO_5 phases.

The microstructure of the directionally solidified Al_2O_3 - $Al_6Ti_2O_{13}$ and $Al_6Ti_2O_{13}$-Al_2TiO_5 eutectic materials were controlled by the thermodynamic conditions imposed by the Al_2O_3 - TiO_2 phase diagram and kinetic conditions of processing. Discussion introduces the description of $Al_6Ti_2O_{13}$ phase, describes the orientation relationships between the $Al_6Ti_2O_{13}$ - Al_2TiO_5 phases and stability of phases. An outline of modified phase diagram for the alumina rich side of Al_2O_3-TiO_2 system is presented and growth morphology is discussed.

4.1. Characteristics of the new $Al_6Ti_2O_{13}$ Phase

Fast solidification and steep temperature gradients, imposed by laser heated floated zone method, produced conditions for quenching of a high temperature aluminium titanate phase of molar composition $Al_6Ti_2O_{13}$. The crystal system is orthorhombic and cell parameters are a = 3.65 Å , b = 9.4 Å , c = 12.5 Å as determined by TEM.

These results are in agreement with the work of Göbbels and Boström [16]. They described the growth of single crystal of aluminium titanate phase from the melt and suggested the molar formulae corresponding to $Al_6Ti_2O_{13}$ as determined by electron microprobe analysis. The structure of this crystal, studied by X-ray diffraction was reported to be monoclinic, space group C2 with cell parameters a=3.635 Å, b=9.312 Å, c=12.469 Å and β=90.04°. Although TEM does not allow cell parameters to be determined with the same precision as by x-ray diffraction methods, values calculated in present investigation are consistent with those presented by Göbbels and Boström. The structure described by these authors was built by five different octahedra, from which four were occupied either by Al or Ti and one octahedron was occupied only by Al. These octahedra were linked by their edges along the c-axis and strongly distorted. The $Al_6Ti_2O_{13}$ structure was therefore derived from the pseudo brookite structure by the insertion of an additional octahedron in the double chain running along the c-direction.

By the time of the writing of this article Norberg et al [18] proposed a refined structure for $Al_6Ti_2O_{13}$. The compound was obtained by solidification using an arc-imaging furnace. They indicated an orthorhombic structure, space group, Cm2m, with cell parameters a=3.65 Å, b=9.368 Å, c=12.555 Å. The structure consists of infinite double chains of polyhedra running along the c axis. These chains are built up by four oxygen octahedra, strongly distorted and randomly occupied by either Ti or Al, as in the structure suggested by Göbbels et al. These two structures differed only in the additional sites that are occupied by aluminum cations. The octahedron in the structure proposed by Göbbels et al. was replaced by a trigonal bipyramid in the structure that has been proposed recently by Norberg et al. Simulation of HREM images of $Al_6Ti_2O_{13}$ structure are currently being calculated and our future work will compare the experimental images from the structural study to validate the formation of this structure.

4.2. Orientation Relationship and Intergrowth of $Al_6Ti_2O_{13}$ and Al_2TiO_5 Phases

The crystals of $Al_6Ti_2O_{13}$ and Al_2TiO_5 are built by double chains of polyhedra along the c axis and have very close values for the a and b cell parameters. As a result, two cells could bond on their (001) faces with almost no atomic displacements as illustrated in Fig 17. This favors the development of (001) interfaces and allows a high degree of intergrowth during solidification as will be described.

The solidification of the Al-Ti-O melt at the 43.9 mol % TiO_2 composition produced two phases, $Al_6Ti_2O_{13}$ and Al_2TiO_5. The *a-, b-, and c- axes of* $Al_6Ti_2O_{13}$ and of Al_2TiO_5 phases were aligned systematically and the cooperative growth axis was parallel to the [100] direction for both $Al_6Ti_2O_{13}$ and Al_2TiO_5 phases. The lamella long interfaces corresponded to (001) planes of both phases.

In the off-eutectic compositions $Al_6Ti_2O_{13}$ / Al_2TiO_5 interfaces were not systematically parallel to (001), but could adopt random orientations. Contrary to what was obtained in the eutectic sample, the Al_2TiO_5 phase was not formed during the solidification but rather it formed by eutectoid reaction at the $Al_6Ti_2O_{13}/Al_2O_3$ interface region during the cooling as will be discussed below. The direction of $Al_2TiO_5/Al_6Ti_2O_{13}$ interfaces was therefore strongly influenced by the direction of the $Al_6Ti_2O_{13}/Al_2O_3$ interfaces formed during the solidification. However, the cells of the two aluminum titanate phases ($Al_6Ti_2O_{13}$ and Al_2TiO_5) were well aligned in both the off eutectic samples as in the eutectic composition sample.

The TEM and HRTEM observations in off-eutectic and eutectic compositions showed that single cells of Al_2TiO_5 were inserted between $Al_6Ti_2O_{13}$ cells by intergrowth in the [001] direction as illustrated in Fig 13 and 14. The intergrowth for sample with 26 mol % of TiO_2 was non periodic and less frequent than the sample with eutectic composition (43.9 mole % of TiO_2). In the eutectic sample a periodicity of one Al_2TiO_5 cell for five $Al_6Ti_2O_{13}$ cells ("1:5") was revealed. The theoretical average composition of a 1:5 intergrowth was calculated in **Table 1**. The measured titanium content was slightly larger than for nominal $Al_6Ti_2O_{13}$ composition (solid line in Fig. 3). This slight excess of Ti that was originally interpreted as being within the uncertainty of WDX measurement but this degree of off-stoichiometry could be accommodated by intergrowths (Table 1).

Mazerolles et al. [17] reported the intergrowth characteristic between pseudobrookite and related phases for various compositions in the region of 30 to 50 mol% of TiO_2. They observed two phases with almost the same a- and b-parameters as Al_2TiO_5 but c parameters were different for each phase, c ~ 1.24

nm and *c* ~ 1.68 nm. The molar formulae of these phases were not specified. Intergrowth between the pseudobrookite and the two related phases were reported. Along [001], blocks of Al_2TiO_5 alternated with blocks of the related phases. Various periodicity in the sequences of stacking were described giving rise to superstructures with c parameters of 3 nm, 8 nm or larger. Norberg et al. [18] have studied multiple crystalline fragments of $Al_6Ti_2O_{13}$ by x-ray diffraction, and could not detect the third phase with c=1.68 nm. However, These authors did not exclude the formation a very small volume of an Al-richer compound, undetectable by x-ray diffraction. In the processing conditions and range of compositions studied in the present work, a third phase with c=1.68 nm was not detected. The volume of material investigated by TEM is however not sufficient to exclude possible formation of this phase.

4.3. Eutectoid Decomposition

$Al_6Ti_2O_{13}$ is a high temperature phase and was maintained as a metastable phase by fast cooling rate used in present work. $Al_6Ti_2O_{13}$ decomposes by the following eutectoid reaction:

$Al_6Ti_2O_{13} \rightarrow Al_2O_3 + 2Al_2TiO_5$ (Eq. 2)

In the as grown samples with 11 and 26 mol % of TiO_2 compositions, a thin layer of Al_2TiO_5 was detected between of Al_2O_3 and $Al_6Ti_2O_{13}$. This suggests that the eutectoid decomposition reaction could take place during cooling only along the alumina dendrites. The alumina dendrites provided energetically favourable sites for the exsolution of Al_2O_3 from the $Al_6Ti_2O_{13}$ phase on fast cooling. In the as grown sample with the 43.9 mol % TiO_2 composition, the $Al_6Ti_2O_{13}$ and Al_2TiO_5 enclosed each other like interlocking microstructure and Al_2O_3 was not expected to form during the solidification. Fast cooling below eutectoid decomposition temperature did not produce Al_2O_3 due to absence of Al_2O_3 seed that could provide lower energy barrier for the eutectoid decomposition of $Al_6Ti_2O_{13}$.

The temperature of 1400 °C was sufficient to produce significant reaction in the interdendritic region for off eutectic compositions. Al_2O_3 dendrites acted as a nucleation site for the eutectoid decomposition during post heat treatments as well as during the fast cooling. In sample with 11 mol % TiO_2 composition annealed at 1500°C for 10 hours, the distance between two dendrites (~2 μm) was short enough to allow the diffusion of all exsoluted aluminum cations to Al_2O_3 dendrites. The dendrites grew and some came into contact. No nucleation of stand-alone alumina precipitates was observed between the dendrites. Interdendritic regions contained only Al_2TiO_5 grains. In sample with 26 mol % TiO_2 composition the distance between dendrites was too long to permit a diffusion of all Al^{3+} towards Al_2O_3 dendrites and thus Al_2O_3 precipitates were formed in distance of a few micron from these dendrites within Al_2TiO_5. Al_2TiO_5 next to Al_2O_3 dendrites was mostly free of Al_2O_3 precipitates, **Figs. 15 and 16b.** As-grown sample with 43.9 mol % TiO_2 composition consisted of Al_2TiO_5 and $Al_6Ti_2O_{13}$ lamellae and did not contain any Al_2O_3. Annealing caused the growth of Al_2TiO_5 lamellae that come into contact with each other. Al_2O_3 nucleated and grew between these lamellae.

As-grown samples were dark blue for 11 m % TiO_2, blue for 26 mol % TiO_2 and black for 43.9 mol % TiO_2 compositions. Ti has low ionization potential and thus can have different valence states in different oxygen partial pressure causing different colors. Although the solidification was carried out in air, the solidification rates were very high and the system was far from equilibrium. During the post heat treatments outer rim regions turned to white in 10 min at 1400°C whereas phase distribution did not change. The effect of the Ti oxidation state on the formation of the non-equilibrim phases is not studied in present work and requires further investigation.

4.4. Modification of Phase Diagram

Previously published phase diagrams of Al_2O_3 - TiO_2 system may be summarized in three different groups with regard to Al_2TiO_5 phase formation. The first group [8, 9] shows an eutectic between Al_2TiO_5 and Al_2O_3 phases approximately 44 mol % TiO_2 and at eutectic temperature of 1850 °C. The Al_2TiO_5 phase crystallises in the pseudobrookite form that is stable up to temperature of 1300 °C below which it decomposes into Al_2O_3 and TiO_2 phases. The second group [10 ,22] exhibits an eutectic point between Al_2TiO_5 and Al_2O_3 phases as that of the first group. However, two allotropic forms of aluminum titanate are reported and described as alpha and beta Al_2TiO_5. The alpha Al_2TiO_5 is a high temperature form which crystallises from the melt and transforms to the stable beta or pseudobrookite form at 1820 °C [10] or 1727 °C [22]. The characterization of the α-Al_2TiO_5 was not possible due to the impracticality of maintaining this form at room temperature. The exception to all of these above mentioned phase diagrams was the work by D. Goldberg [23, 24]. He presented outlines of a phase diagram that does not show any

eutectic structure in the alumina rich part. Goldberg reported that specimens grown from the melt in the alumina rich part of the phase diagram were composed of at least two alumina rich aluminum titanate phases and he described these phases as α' phases. The x-ray pattern of the α' phases and optical micrographs of the eutectoid reactions brought evidences for these high temperature phases but no further characterization and analysis were presented. None of these phase diagram studies were associated with microstructural characterization and orientation relationship in the polyphase structures.

Based on the microstructural understanding for the development of the Al_2O_3, Al_2TiO_5 and $Al_6Ti_2O_{13}$ phases, it was possible to re-examine the phase diagram of the Al_2O_3 rich side of Al_2TiO_5 - Al_2O_3 eutectic and compare with the previously published phase diagrams. Al_2TiO_5 - Al_2O_3 eutectic structure did not solidify between Al_2O_3 dendrites for the 11 and 26 mol % TiO_2 compositions. This is contrary to what was predicted by previously published phase diagrams described above**.** At the eutectic invariant point (43.9 mol % TiO_2) the absence of the Al_2O_3 phases was noteworthy given that Al_2O_3 is a very stable phase. Moreover, a high temperature aluminum titanate phase, richer in alumina than Al_2TiO_5 could be maintained at room temperature as described by Goldberg [24]. **Figure 18** presents the outline of a phase diagram based on the structural and chemical characterization of this work. A deeper thermodynamical analysis and phase equilibrium study will be required to determine the exact temperatures and compositions of the phase boundaries.

A vertical segment at 40 mol % is added on this outline of phase diagram which represents the high temperature $Al_6Ti_2O_{13}$ phase between ~1850 and ~1800°C. The introduction of this new compound induces the insertion of a invariant point on the liquidus, that can be either a eutectic point at less than 40 mol % TiO_2 or a peritectic point at more than 40 mol% of TiO_2. At the eutectic point, $Al_6Ti_2O_{13}$ and Al_2O_3 would solidify simultaneously whereas at the peritectic point the liquid would react with alumina to form $Al_6Ti_2O_{13}$. The TEM and HRTEM observations permit to choose between these two hypotheses. In the case of a eutectic point the samples AT11 and AT26 would consist of an alumina primary phase surrounded by $Al_6Ti_2O_{13}$ and Al_2O_3 eutectic matrix. No alumina domains have been observed by TEM and HRTEM in the $Al_6Ti_2O_{13}$ matrix. The hypothesis of a peritectic reaction involves a liquid richer in titania than $Al_6Ti_2O_{13}$ and requires the migration of Ti and O ions from this liquid into alumina and the transformation into $Al_6Ti_2O_{13}$. This mechanism requires solid diffusion of the ions into alumina crystal and thus it may be kinetically prohibited. The fast solidification rates used in this work might be incompatible with a total consummation of the excess Ti cations in the liquid by the peritectic reaction to attain the $Al_6Ti_2O_{13}$ composition. The HRTEM observations of sample AT26 have revealed a small level of intergrowth of Al_2TiO_5 between $Al_6Ti_2O_{13}$. This intergrowth demonstrates that solidification of a liquid richer in titania than $Al_6Ti_2O_{13}$ formed. The chemical shift was balanced by the crystallization of Al_2TiO_5, phase richer in titania than $Al_6Ti_2O_{13}$. The high degree of resemblance between Al_2TiO_5 and Al_2TiO_5 structures render this intergrowth as energetically favourable. The low density of intergrowth in AT26 matrix supports a peritectic point close to $Al_6Ti_2O_{13}$.

The sharp minimum in the liquidus temperature at around 43.9 mol % TiO_2, which was first measured by Bunting [9] was previously interpreted as an invariant eutectic point between Al_2TiO_5 and Al_2O_3. The insertion of the $Al_6Ti_2O_{13}$ compound in the phase diagram between Al_2TiO_5 and Al_2O_3 modifies the constituent phases of the eutectic region which must be formed between $Al_6Ti_2O_{13}$ and Al_2TiO_5. This suggestion is further supported by the structural analysis of sample solidified from a melt with 43.9 mol % TiO_2 composition. The rapid solidification did not produce Al_2O_3 and Al_2TiO_5. Lamellae of Al_2TiO_5 were separated by an aluminium titanate superstructure formed by an intergrowth between $Al_6Ti_2O_{13}$ and Al_2TiO_5. The average composition of this superstructure was very close to that of $Al_6Ti_2O_{13}$. It is likely that the composition of sample 43.9 mol % TiO_2 was not strictly that of the $Al_6Ti_2O_{13}$ - Al_2TiO_5 eutectic but slightly richer in TiO_2. The eutectic invariant point has been placed around 43.5 mol % TiO_2 as shown in Fig. 18. This small difference in composition was accommodated by the intergrowth of Al_2TiO_5. Another possibility that requires discussion is that Al_2TiO_5 solidified first leaving a eutectic liquid of composition close to 5 $Al_6Ti_2O_{13}$: 1Al_2TiO_5. This is unlikely because the eutectic would be almost superimposed with the peritectic.

4.5 Growth Morphology

In the off-eutectic compositions, 12 and 26 mol % TiO_2, the volume fractions of primary dendrites in the outer rims were higher than in the core region (**Figs. 4c, 5b**). This feature was extreme for the 26 mol % TiO_2 composition, in which most dendrites were practically in contact with each other (**Fig. 5b**). The

rate of heat removal from the molten zone surface at the liquid-solid interface is considerably higher than in the interior which produces the observed microstructural differences. The solidification reaction of this system can be further explained by considering the kinetics of the process and nucleation frequency of the Al_2O_3 phase. The effect of concentration of Al_2O_3 dendrites at the outer rim region to build a skin layer is twofold. First, the large central region is composed of smaller Al_2O_3 dendrites since the overall composition of the liquid is richer in titanium and microstructure adapts to reflect the compositional modification. Second, the mechanical properties are strongly affected from the formation of rim region containing primarily Al_2O_3 dendrites as has been discussed in an accompanying report [15]. The comparison of microstructures obtained at compositions at 11 and 26 mol % TiO_2 convey additional information about the Al_2O_3 dendrites. Unlike the process of lamellar growth, the Al_2O_3 dendrites do not grow exactly normal to the moving interface and not exactly parallel to each other either. The Al_2O_3 dendrites diverge as they solidify as shown in **Figs. 4a** and **5a** and grow in direction of local gradient maximum. If the interphase spacing between Al_2O_3 dendrites becomes greater than that of the imposed growth rate, a new Al_2O_3 dendrite has to nucleate in the region between them. Conversely, if two Al_2O_3 dendrites approach each other on the interface, one phase must be terminated due to an insufficient supply of cations in the liquid, for example Al^{3+}. The thickness and lateral spacing of the Al_2O_3 dendrites was determined by the growth rate, and their length was determined by the convergence of two phases at the interface. This representation was in agreement with the SEM observations in Figs. 4 and 5, so that solidification was a constantly repeating cycle of nucleation of Al_2O_3 dendrites whenever necessary to keep the interphase spacing at the required value. The $Al_6Ti_2O_{13}$ phase, which solidifies between the primary dendrites keep the [100] direction as growth axis whereas the dendrites change their orientations with respect to the growth axis. Therefore, no systematic orientation relationship was observed between $Al_6Ti_2O_{13}$ and Al_2O_3. In addition, the Al_2TiO_5 layer formed at $Al_6Ti_2O_{13}/Al_2O_3$ interfaces during cooling has the tendency to follow the curved surface of the dendrites as seen in Fig 5c and 7. As a result, the interfaces separating Al_2TiO_5 and $Al_6Ti_2O_{13}$ could adopt random orientations although the cells of the two aluminum titanate were aligned.

The solidification characteristic of Al_2O_3 - $Al_6Ti_2O_{13}$ system for the AT26 (26 m % TiO_2) composition was controlled more by the efficacy of heterogeneous nucleation centers in the liquid than by any other factors. Under the fast solidification conditions applied in the present investigation, Al_2O_3 dendrites grew ahead of the liquid, as it is apparent from the formation of well developed Al_2O_3 dendrites (Fig. 5). An increase of TiO_2 content for the AT11 (11 m % TiO_2) decreased the extension of dendrites into the liquid as observed from SEM micrographs of longitudinal sections revealing short dendrites. To understand the shortening of the Al_2O_3 dendrite length, it is more pertinent to compare the temperature gradient for the different compositions. An increase of TiO_2 concentration required a larger amount of heat to melt an equivalent amount of molten zone compared to Al_2O_3 rich region. The additional amount of heat requirement for increased TiO_2 content was an indication for the modification of the thermal gradient in radial and axial direction of the molten zone. This alteration of the thermal gradient also contributed for the shortening of the Al_2O_3 dendrite length.

The lamellae morphology is produced during the directional solidification from a melt of 43.9 % TiO_2 (close to eutectic invariant point). The width of the lamellae is fixed by the growth rate and thermal gradient. These lamellae are arranged into colonies. The colonies have their *a* directions parallel to the growth axis and rotations of the *b* and *c* directions were observed from one colony to the other. The absence of cracks at the lamellae interfaces indicated similar coefficient of thermal expansion of the $Al_6Ti_2O_{13}$ and Al_2TiO_5 phases and no thermal mismatch occurred if the phases were oriented the same way. Each colony can be considered as a single crystal entity as far as their thermal expansion behavior is concerned. However, the strong difference in the α_b and α_c coefficient leads to a decohesion at the colony boundaries as illustrated in **Figure 1b.**

Summary of Results and Conclusions

Directional solidification characteristics of Al_2O_3-TiO_2 melts with11, 26, 43.9 mole % of TiO_2 content were investigated using laser heated float zone method. Based on microstructural characterization using XRD, WDX, SEM, HRTEM and STEM-EDX analyses we had the following conclusions.

- No Al_2O_3-Al_2TiO_5 eutectic was formed for any compositions studied. Even though, previous phase diagrams suggests formation of Al_2O_3-Al_2TiO_5 eutectic for 43.9 mol. % TiO_2 and formation of primary Al_2O_3 dendrites for off eutectic compositions, 11 and 26 mol % TiO_2.
- An additional phase $Al_6Ti_2O_{13}$ was crystallized that was not previously predicted by the phase diagrams. The $Al_6Ti_2O_{13}$ phase have *a* and *b* parameters analogous to that of Al_2TiO_5 and *c* was equal to ~5/4 that of Al_2TiO_5. Alignment of the $Al_6Ti_2O_{13}$ and Al_2TiO_5 cell base vectors was systematically observed.
- The solidification of the 11 and 26 mol.% TiO_2 melt produced alumina primary dendrites separated by $Al_6Ti_2O_{13}$ matrix. An Al_2TiO_5 interphase was formed during fast cooling between $Al_6Ti_2O_{13}$ and Al_2O_3 from the $Al_6Ti_2O_{13}$ matrix. The solidification of the 43.9 mol. % TiO_2 produced a lamellae structure composed of Al_2TiO_5 and an aluminum titanate superstructure that consist of intergrowth in the [001] direction (one Al_2TiO_5 cell for five $Al_6Ti_2O_{13}$ cells).
- Post heat treatment at 1400°C decomposed $Al_6Ti_2O_{13}$ into Al_2O_3 and Al_2TiO_5 by a eutectoid reaction. This solid-state reaction could not take place during laser processing of the materials due to the rapid cooling rates, except locally around alumina dendrites, which offered energetically favourable nucleation sites for the decomposition.
- Based on these observations an outline of a new phase diagram was proposed for the Al_2O_3 rich side of Al_2O_3 – TiO_2 system. Accordingly, line compound $Al_6Ti_2O_{13}$ formed as a high temperature phase at 40 mol.% TiO_2 and defined new phase fields at high temperatures. The eutectic invariant point is at ~ 43.5 % TiO_2 between $Al_6Ti_2O_{13}$ and Al_2TiO_5 phases. A peritectic point was suggested between $Al_6Ti_2O_{13}$ and the $Al_6Ti_2O_{13}$-Al_2TiO_5 eutectic.
- The experimental investigation of directionally solidified structures presented in this work provided an understanding of dendrite or lamellae structures, orientation relationship and crystallography of the interfaces. The morphology for the 43.9 mole % TiO_2 composition can be described as continuous Al_2TiO_5 lamellae surrounded by intergrowth of Al_2TiO_5/$Al_6Ti_2O_{13}$ (~1:5) matrix phase. These were assembled into colonies and grew along [100]. Rotations of [010] and [001] directions were seen from one colony to another. Colony boundaries had cracks due to thermal expansion mismatch. The directions of the Al_2O_3 dendrites principal axes for the 11 and 26 mol. % TiO_2 compositions were not systematically aligned to the growth axis and differed in the same sample. The growth axis of $Al_6Ti_2O_{13}$ matrix was [100].

As a future perspective, these results and proposed modification of phase diagram supplied sufficient knowledge base to elucidate the microstructure of the directionally solidified ceramics in conjunction with the growth conditions that can be further utilized with other systems containing pseudobrookite structure. A general discussion of eutectic phenomena was presented in order to convey that the experimental results can be extended to wide range of systems with microcracked matrix and weak interfaces to engineer strong and tough structural materials. The proposed microcracked toughening mechanism of cellular growth and off-eutectic solidification have not been previously explored for ceramics and may in fact be relevant for other DSE systems.

References

[1] A. Sayir, in Computer-Aided Design of High-Temperature Materials. Eds. A. Pechenik, R.K. Kalia, P. Vashista, *Oxford University Press (1999) pp.197 – 211.*

[2] V. S. Stubican and R. C. Bradt, *Ann. Rev. Mater. Sci.*, **11** 267-297 (1981).

[3] A. Sayir and S. C. Farmer, *Acta Mat.*, **48** 4691 - 4697 (2000).

[4] T. A. Parthasarathy, T. Mah, and L.E. Matson, *J. Amer. Ceram. Soc.*, **76** [1] 29-32 (1993).

[5] A. S. Argon, J. Yi and A. Sayir, *Mat. Sci. and Eng.*, **A319 –321** 838 - 842 (2001).

[6] C. Frazer, E. Dickey and A. Sayir, *J. Crystal Growth*, **232** [1-2] 187- 195 (2001).

[7] L. E. Matson, R.S. Hay, and T. Mah, *Ceram. Eng. Sci. Proc.*, **10** 764 (1989*).*

[8] H. Von Wartenburg and H.J. Reusch *Zeit. Anorg. Allgem. Chem*. **207** 1, (1932)

[9] E.N. Bunting *Bur. Stand. J. Res.* **11** 725 (1933).

[10] S.M. Lang, CL Fillimore, LH Maxwell J. *Res. Natl. Bur. Stds.*, **48**, 298 (1952)

[11] H.A.J. Thomas – R. Stevens Aluminium Titanate – A literature Review- Part I: Microcraking Phenomena.– Br. Ceram. Trans. J. 88, 144-151 1989

[12] S. Bueno, R. Moreno, C. Baudín *J. Eur. Ceram. Soc.* **24** [9] 2785-2791 (2004).

[13] S. Bueno, R. Moreno, C. Baudín *J. Eur. Ceram. Soc* **25** [6] 847-856 (2005).

[14] A. Sayir, M.H. Berger, C. Baudín, *Ceram. Eng. Sc. Proc.* **26** [2] 225-233 (2005.

[15] C. Baudín, A. Sayir and M.H. Berger *Acta Materialia,* **54**, [14] 3835-3841 (2006).
[16] M. Goebbels, D. Bostroem Abstract published in "Berichter der Deutschen Mineralogishen Gesellshaft vol 9 n°1 p128 1997.
[17] L. Mazerolles, V. Bianchi, D.Michel , proceedings of ICEM 13 17-22 July 1994 pp 905 906
[18] S. T. Norberg, S. Hoffmann, M. Yoshimura, N. Ishizawa, Acta Cryst. C61, i35-i38 (2005).
[19] B. Morosin and R.N. Lynch *Acta Cryst.* **B28** 1040 (1972).
[20] Although colony boundaries were very small in comparison to other oxide eutectic structures
[21] D. J. Rowcliff, W. J. Warren, A. G. Elliot and W. S. Rothwell, *J. Mat. Sci.*, **4** 902-907 (1969).
[22] L. Kaufman , Physica B+C **150**[1-2] 99-114 (1988).
[23] D. Goldberg Rev. Int. Hautes Tempér. et Réfract. **5** 181-194 (1968).
[24] D. Goldberg, PhD Thesis CECM Vitry sur Seine, France, 1968

Composition	Al wt %	Ti wt %	O wt %
Al_2TiO_5 (=$2Al_2O_3.1TiO_2$)	29.68	26.33	44.00
$Al_6Ti_2O_{13}$ (=$3Al_2O_3.2TiO_2$)	34.77	20.56	44.67
5 $Al_6Ti_2O_{13}$ / 1 Al_2TiO_5	34.40	20.98	44.62

Table 1 : Nominal compositions in weight % of the aluminum titanates that formed during

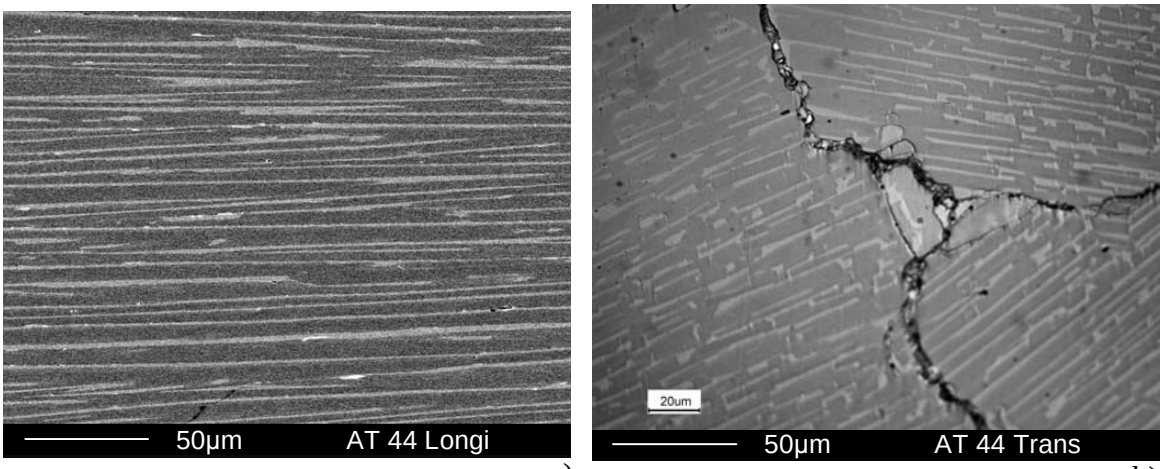

a) b)

Figure 1: Sample AT44 (43.9 mol% TiO_2): a) SEM image of a longitudinal section exhibiting continuous bright lamelae in a dark matrix. b) Optical image of a transverse section showing discontinuous lamellae arranged in colonies of distinct orientations. Cracks separate the colonies.

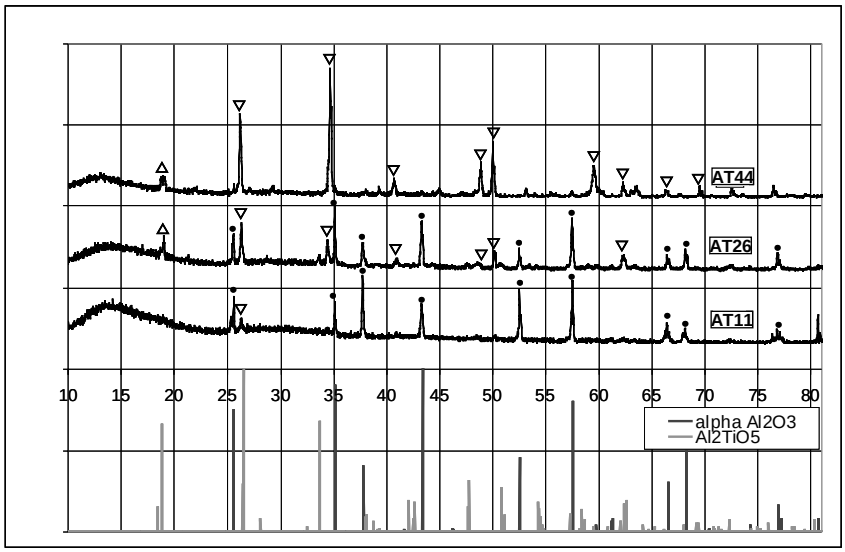

Figure 2: X-ray diffraction spectra of AT44, AT26 and AT11, compared with peak positions of α-Al_2O3 (black lines) and β-Al_2TiO_5 (grey lines JCPDF 41-0258 space groupe Bbmm) Peaks labelled "•" are those of α-Al_2O_3, only the peak labelled "△" could be indexed as 020 (using equivalent space group Cmcm see foot note) of the β-Al_2TiO_5 phase those labelled "▽"show significant shift from the β-Al_2TiO_5 diffraction peaks.

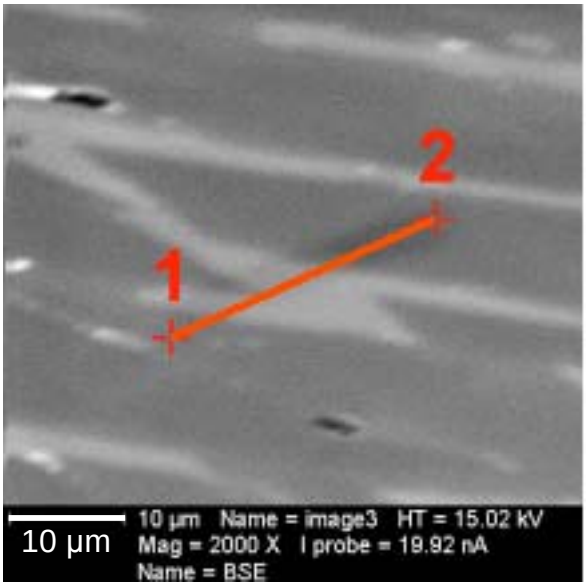

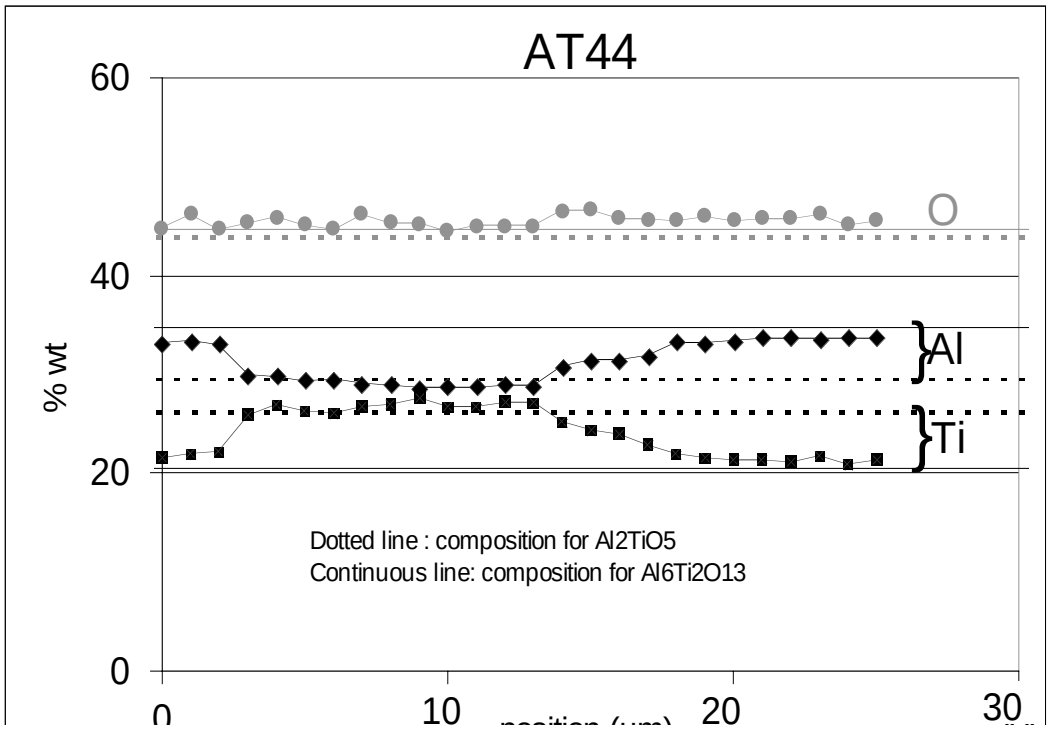

Figure 3 :WDX profile on sample AT44 measured between points 1 and 2 on top SEM image. Symbols indicate measurements for O (●), Al (♦) and Ti (■). Horizontal lines correspond to calculated weight percentages in Ti, Al, O for $Al_6Ti_2O_{13}$ (solid lines) and for Al_2TiO_5 (dotted lines)

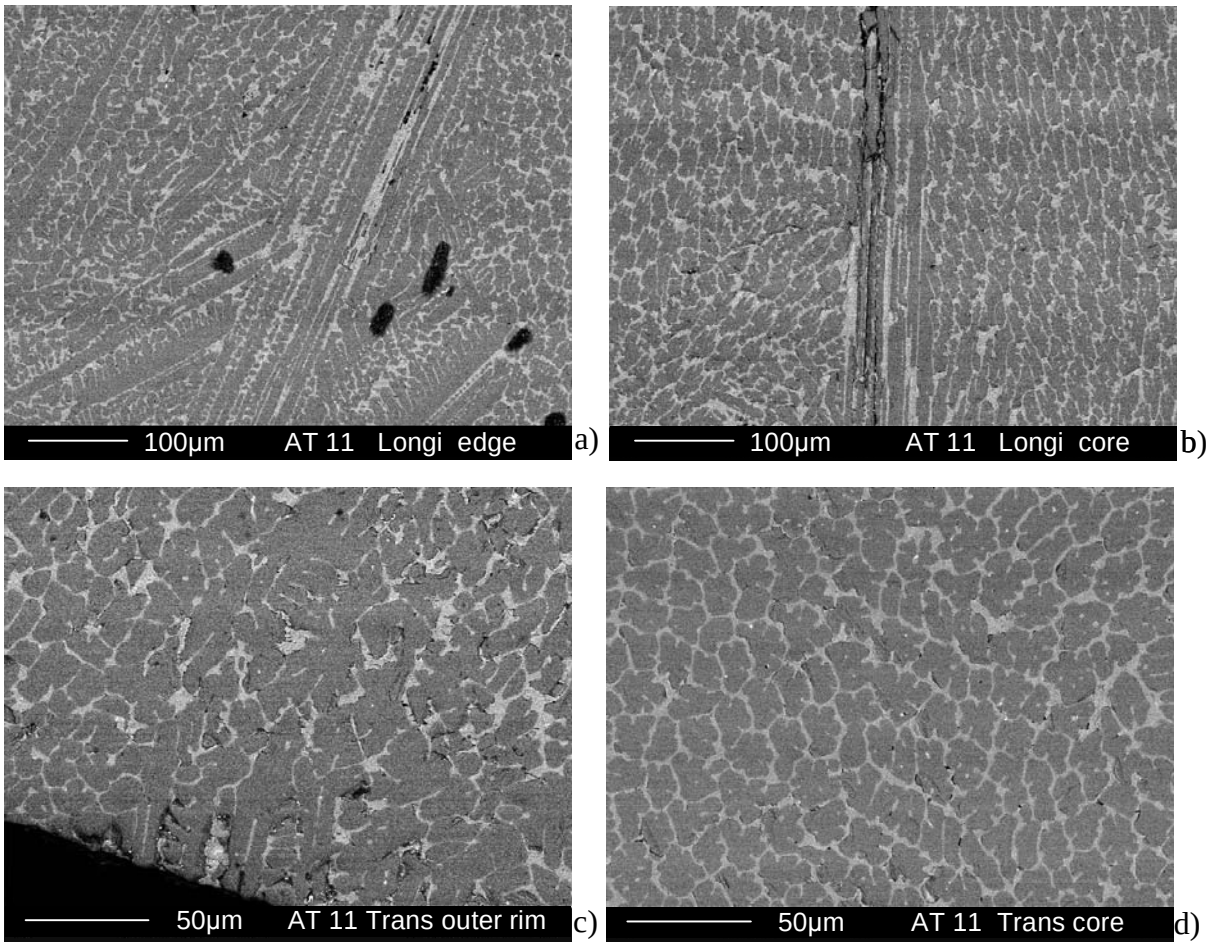

Figure 4: SEM images of sample AT11 (11 mol % TiO_2). a, b) :Longitudinal sections showing variation in the orientation of the dendrites (a) except close to the core of the sample (b) where the dendrites are aligned along the growth axis. c,d) Transverse section showing outer rim with closely packed dendrites (c), and core region (d).

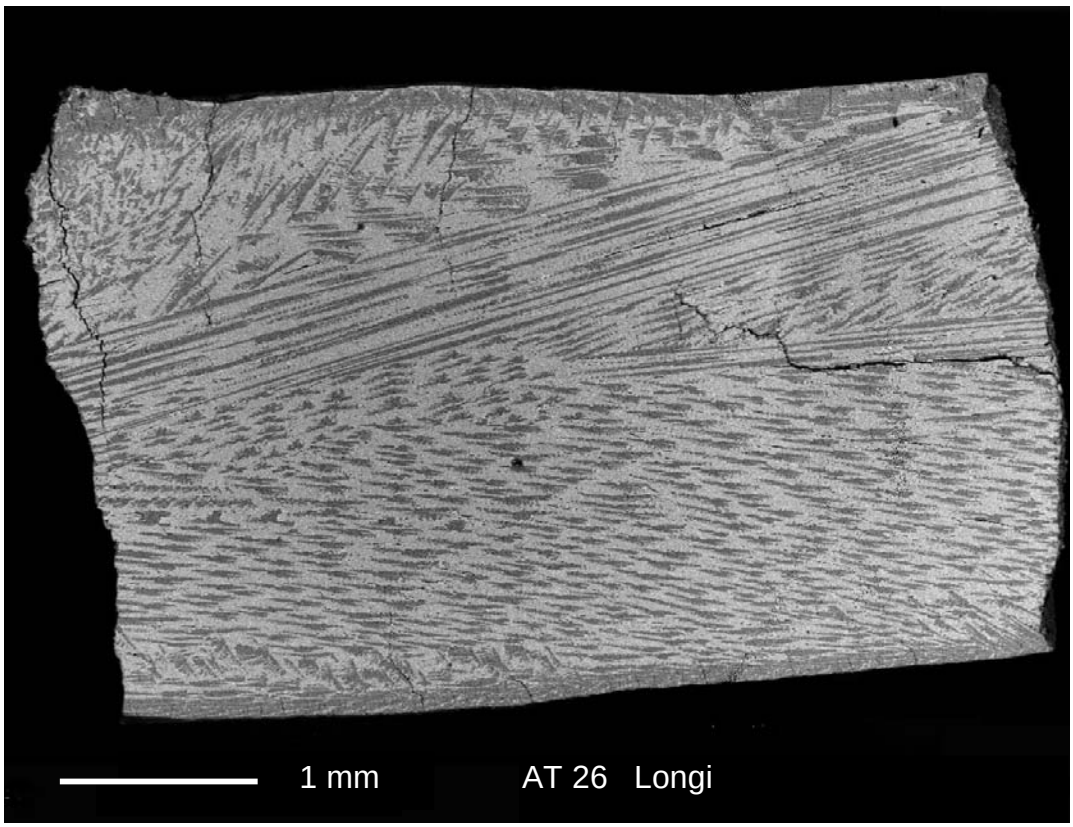

a)

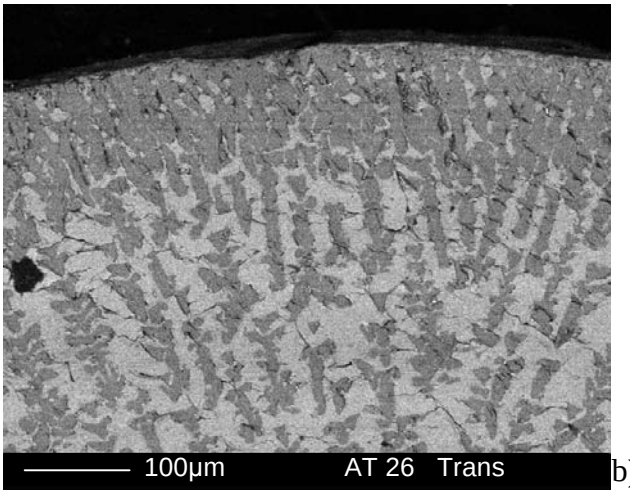

b)

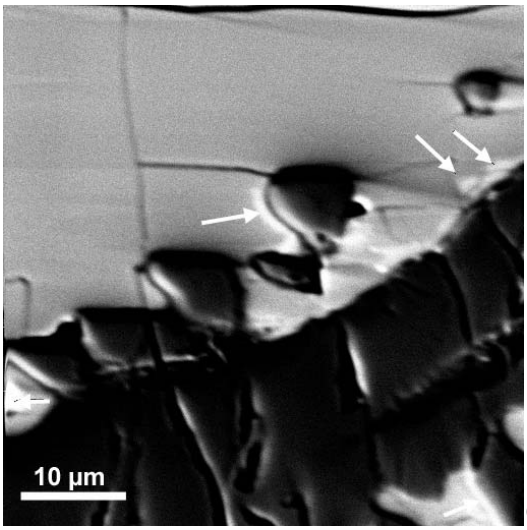

c)

Figure 5: SEM images of sample AT26 (26 mol % TiO_2) a) longitudinal and b) transverse sections showing closely packed dendrites in the outer rim an variation of the orientation of the dendrites. c) A whiter interphase is observed (arrows) between dendrites and matrix.

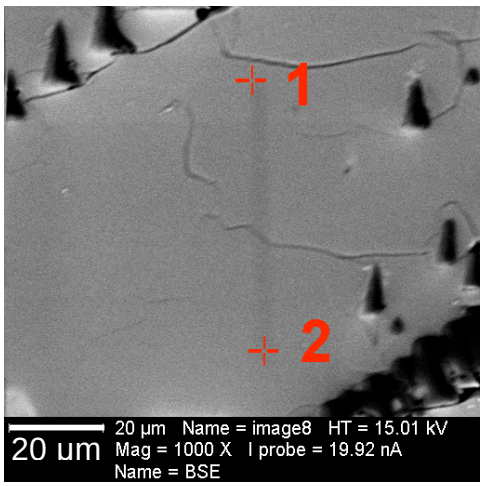

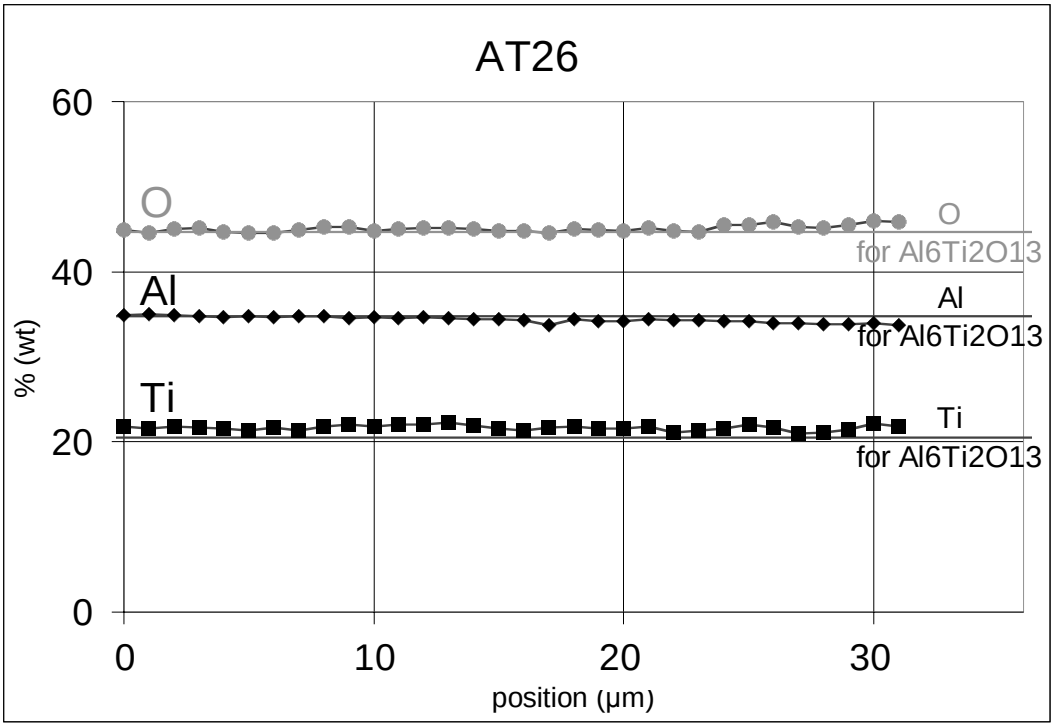

Figure 6 WDX profile on sample AT26 measured between points 1 and 2 on top SEM image. Symbols indicate measurements for O (●), Al (♦) and Ti (■). Horizontal lines correspond to calculated weight percentages in Ti, Al, O for $Al_6Ti_2O_{13}$ (solid lines). The average composition of the Al-Ti-O phase determined by this method was 21 wt % Ti; 35 wt % Al and 45 wt % O, adding up 101 wt %.

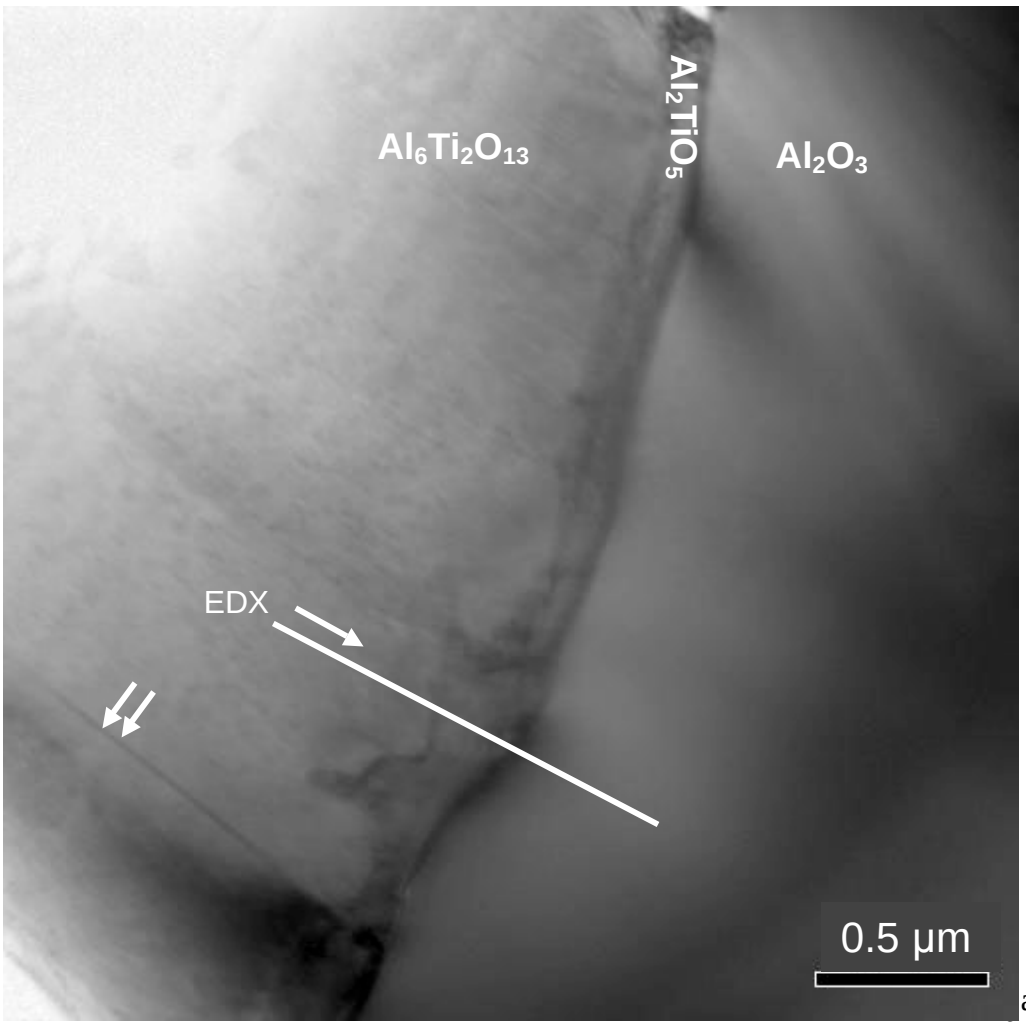

a)

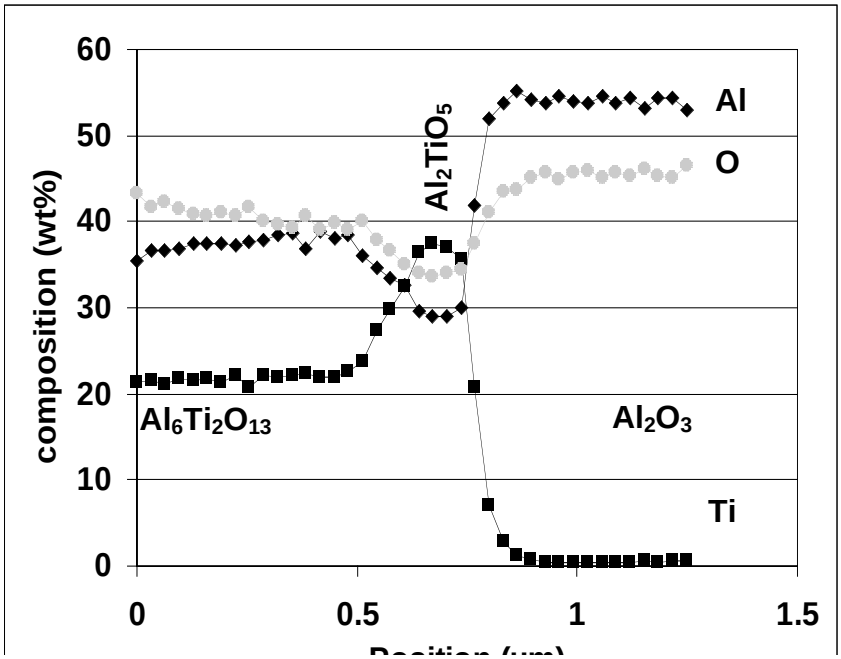

b)

Figure 7 : a) TEM micrograph showing a Al_2O_3 dendrite edge (right) and the $Al_6Ti_2O_{13}$ phase (left) and an interphase. The double arrow locates a region of Al_2TiO_5 intergrowth.
b) STEM-EDX profile recorded on the line shown on the micrograph to follow qualitatively the variations of O (●), Al (♦) and Ti (■) in the interphase region.

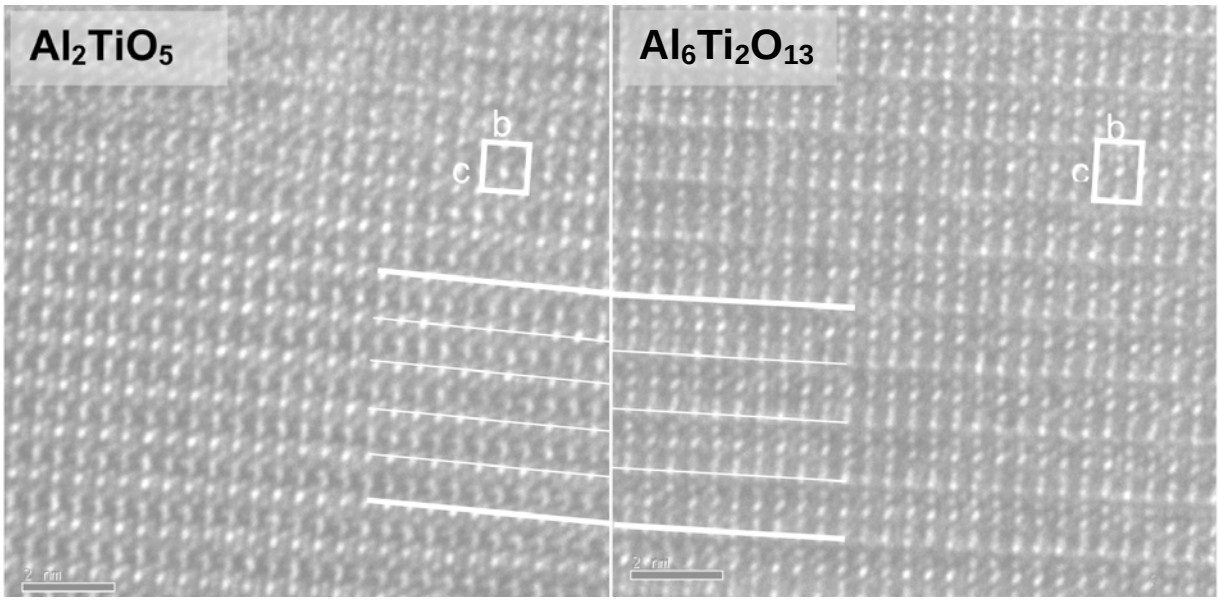

Figure 8: High resolution TEM images of a) Al_2TiO_5 and b) $Al_6Ti_2O_{13}$ both in [100] zone axis. Solid lines illustrate the relation $5d_{001,Al_2TiO_5} \approx 4d_{001,Al_6Ti_2O_{13}}$ c) SAD pattern of $Al_6Ti_2O_{13}$ in [100] zone axis.

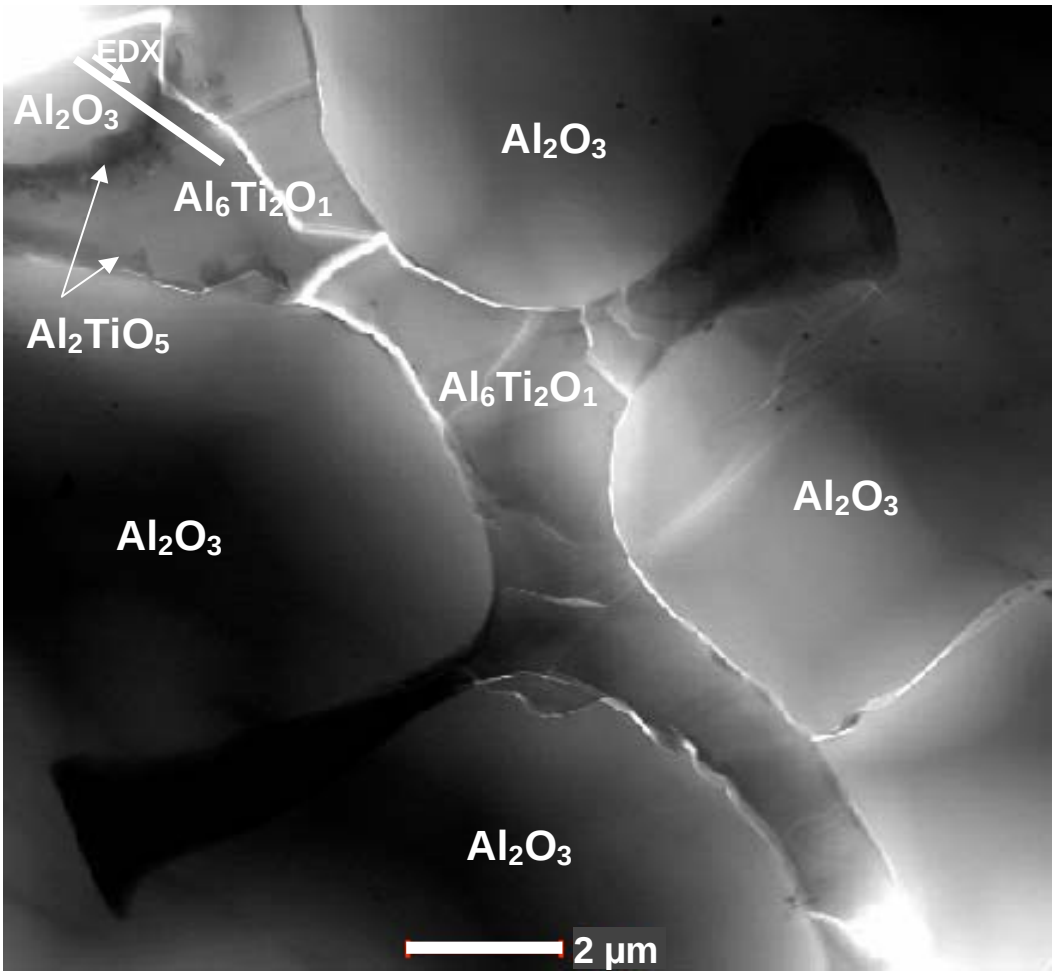

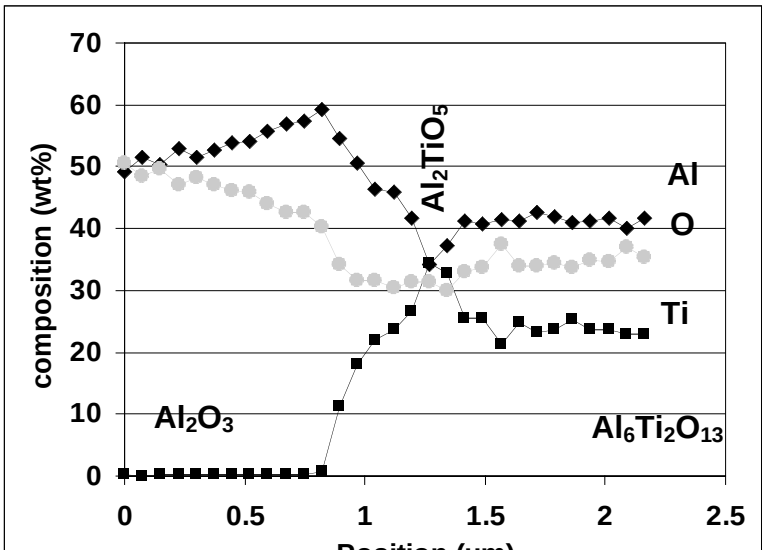

Fig 9: a) TEM image of a cross section of the alumina rich sample AT11. b). The STEM-EDX.

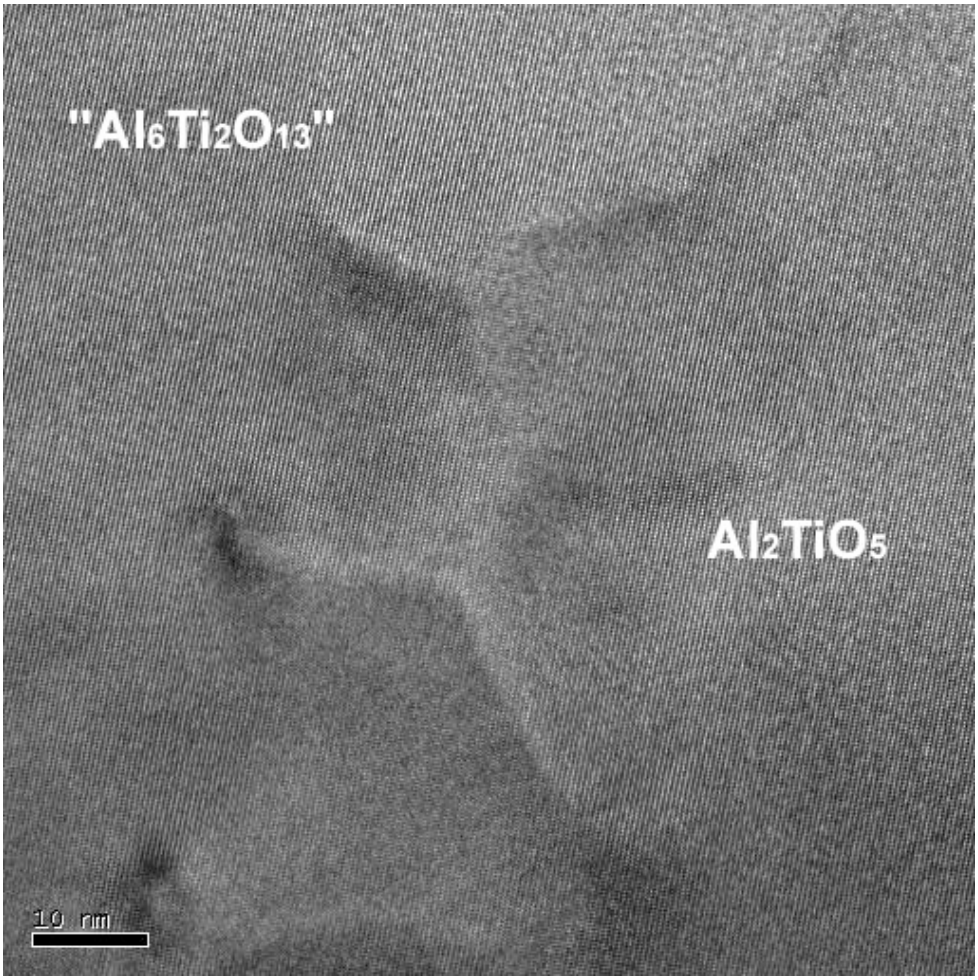

a

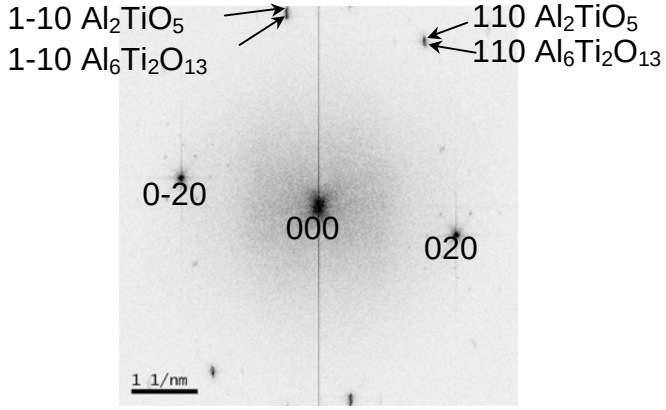

b

Figure 10: (a) High resolution image of AT44 in [001] zone axis across a Al_2TiO_5 and $Al_6Ti_2O_{13}$ interface b) associated FFT: the 110 reflections for Al_2TiO_5 and $Al_6Ti_2O_{13}$ do not overlap.

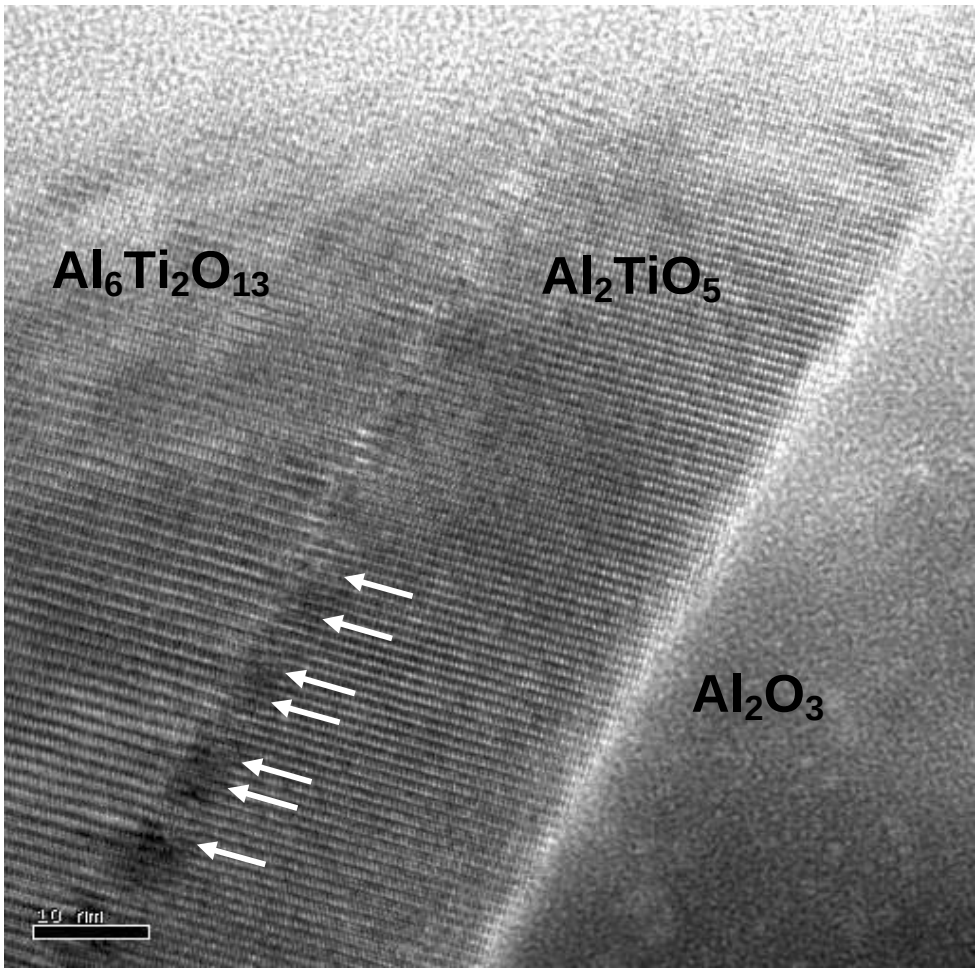

Fig 11 : $Al_6Ti_2O_{13}$ / Al_2TiO_5 /Al_2O_3 region in sample AT26. $Al_6Ti_2O_{13}$ and Al_2TiO_5 are in [100] zone axis. White arrows show (001) planes of Al_2TiO_5 that terminate at the $Al_6Ti_2O_{13}$/Al_2TiO_5 interface to accommodate misfit between inter-reticular distances of (001) planes of the two phases. Other planes are continuous across the $Al_6Ti_2O_{13}$/Al_2TiO_5 interface.

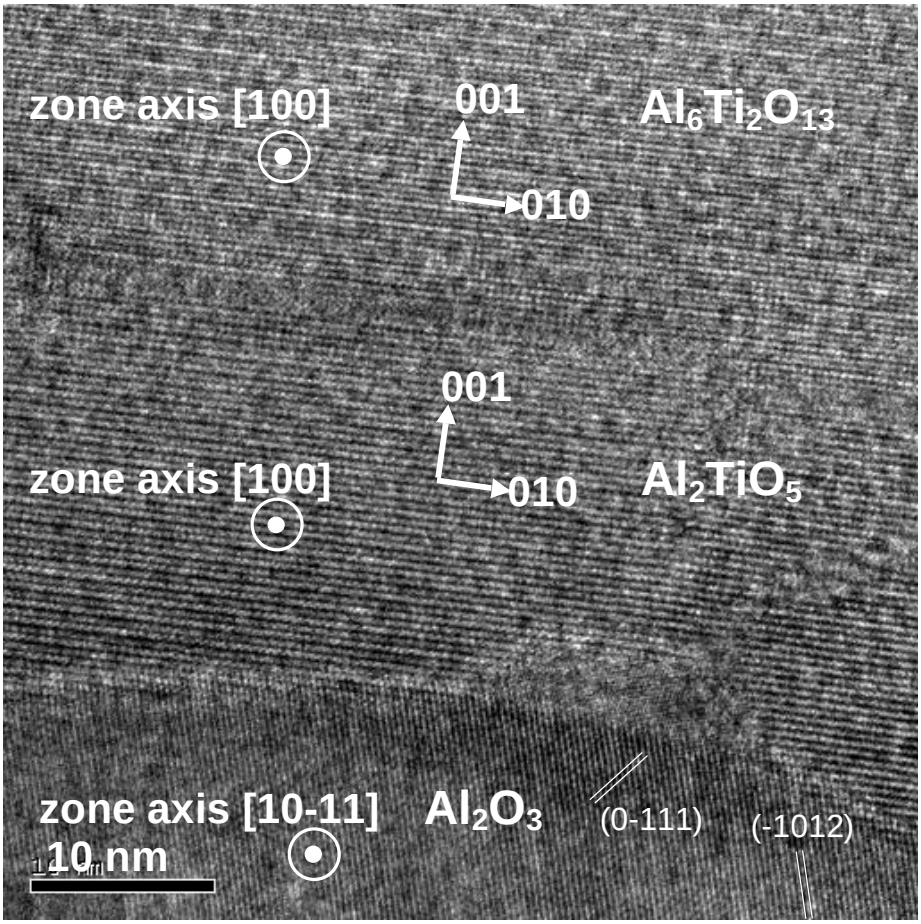

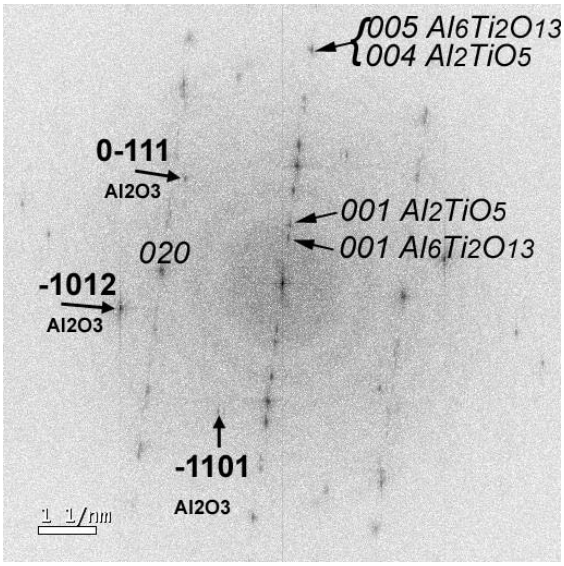

Fig 12: $Al_6Ti_2O_{13}$ / Al_2TiO_5 /Al_2O_3 region in sample AT26 and corresponding FFT pattern. Aluminum titanates are in [100] zone axis and alumina in [10-11] zone axis. Interfaces are curved and not observed edge on.

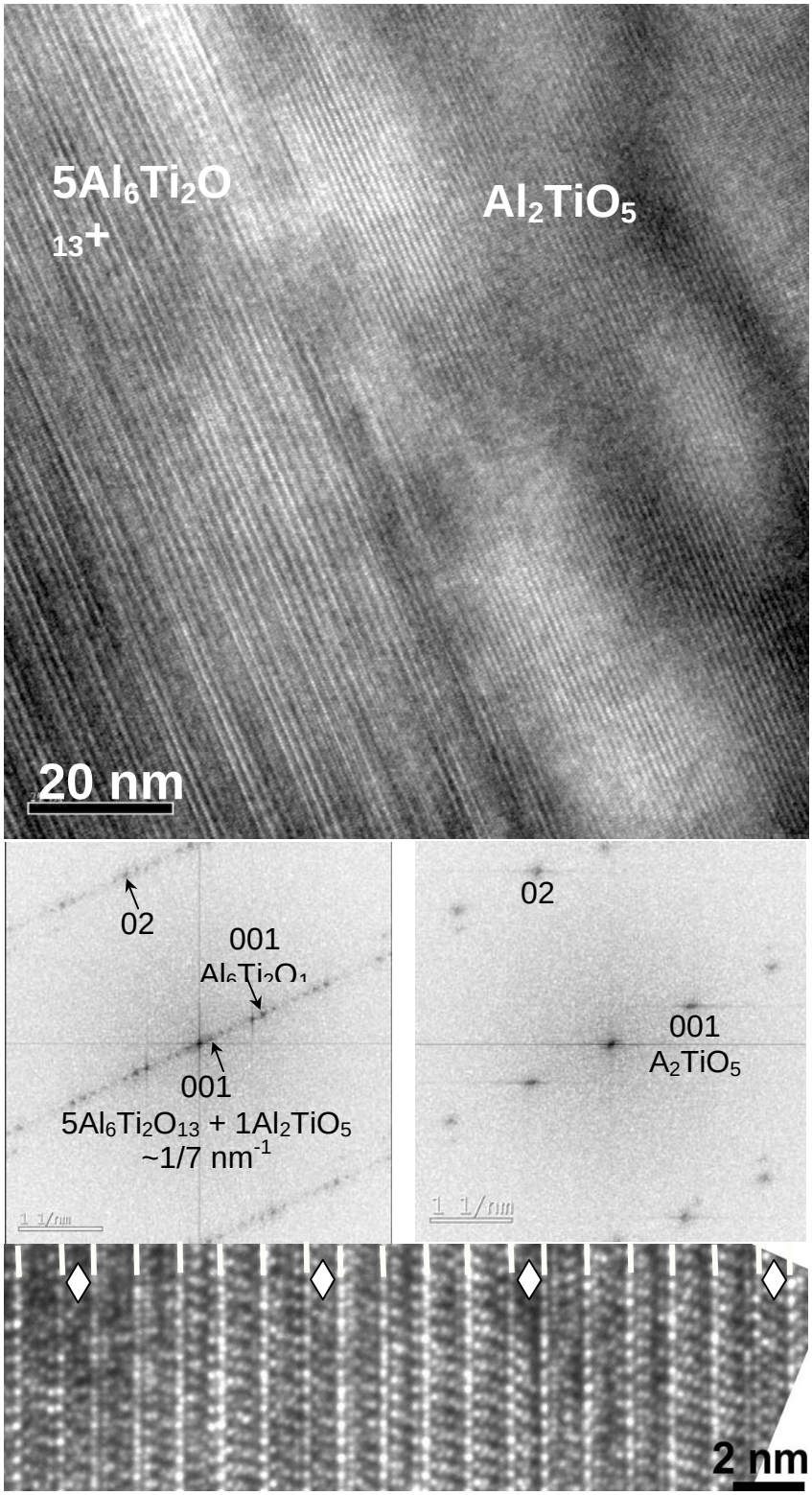

Figure 13: a) Interface region between lamella (right) and matrix (left) in sample AT44 observed in [100] zone axis (= growth axis). b) FTT of the matrix region b) FFT of the lamella region. Intergrowth of Al_2TiO_5 and $Al_6Ti_2O_{13}$ is observed in the matrix region. The FFT shows superlattice reflections at 1/7 nm^{-1} corresponding to a mean periodicity of one block Al_2TiO_5 inserted every five blocks of $Al_6Ti_2O_{13}$. d) detail of the matrix region showing one Al_2TiO_5 block (◇) every fiveor four blocks of $Al_6Ti_2O_{13}$.

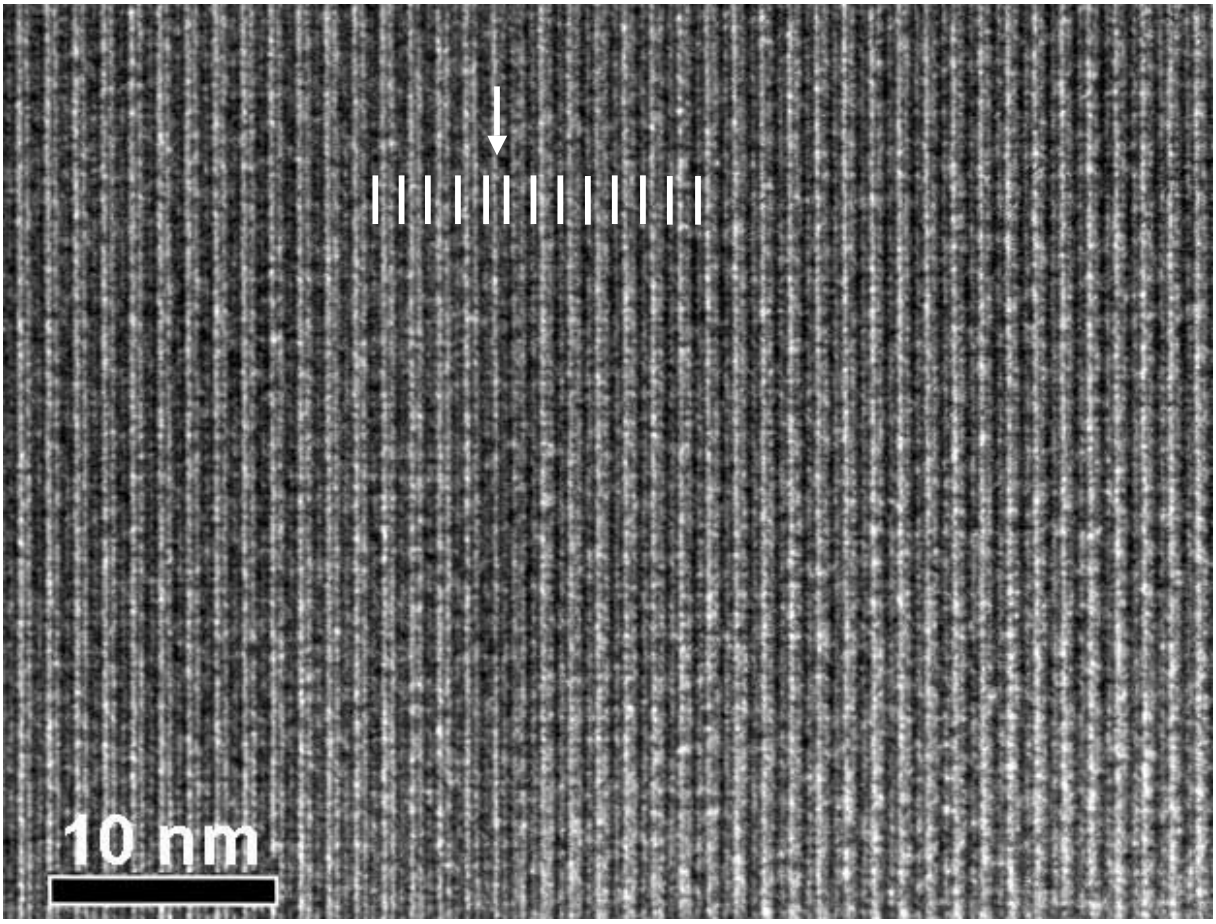

+

Fig 14 : Insertion of a single layer of Al_2TiO_5 (9.6 Å) (arrowed) between $Al_6Ti_2O_{13}$ layers (12.5 Å) matrix in sample AT26.

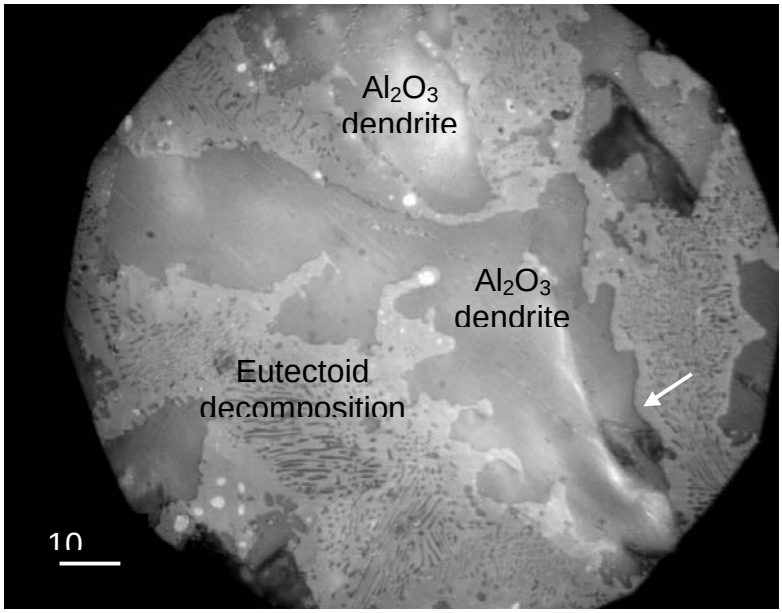

Figure 15 Optical image of sample AT26 annealed for 5 hours at 1400°C: eutectoid reaction occurred in the $Al_6Ti_2O_{13}$ matrix to form Al_2TiO_5 matrix(light grey) and Al_2O_3 precipitates (dark grey). Arrow shows a layer surrounding the dendrite that does not enclose alumina precipitates.

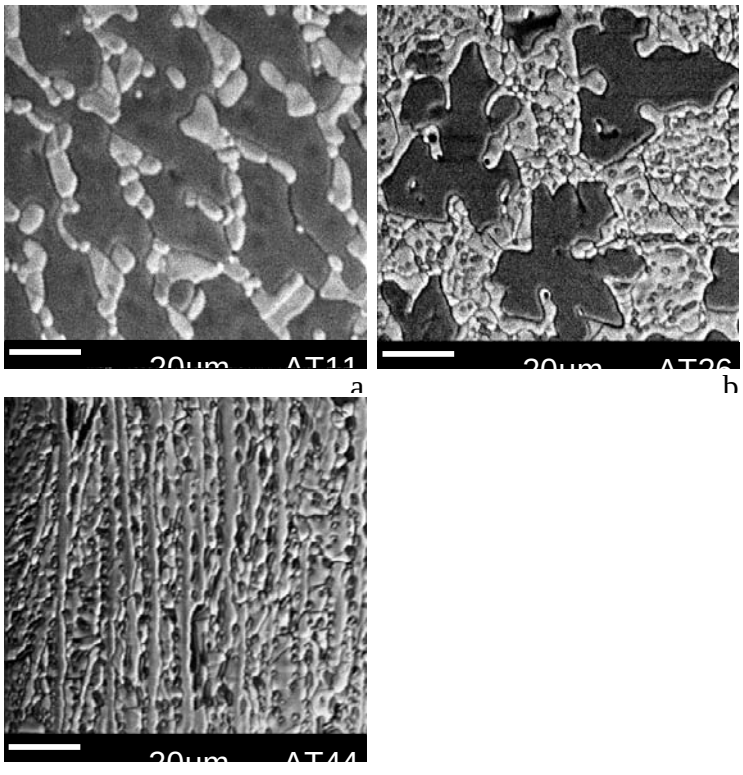

Figure 16 : SEM images of the three compositions annealed for 10 hours at 1500°C. The samples consist of Al_2O_3 (darker phase) and Al_2TiO_5 (brighter phase). a) AT11: Al_2TiO_5 grains between Al_2O_3 dendrites. b) AT26: Al_2O_3 dendrites, Al_2O_3 precipitates included in Al_2TiO_5 phase. c) AT44: Al_2TiO_5 lamellae in contact to each other, precipitates of Al_2O_3 aligned in rows parallel to the Al_2TiO_5.

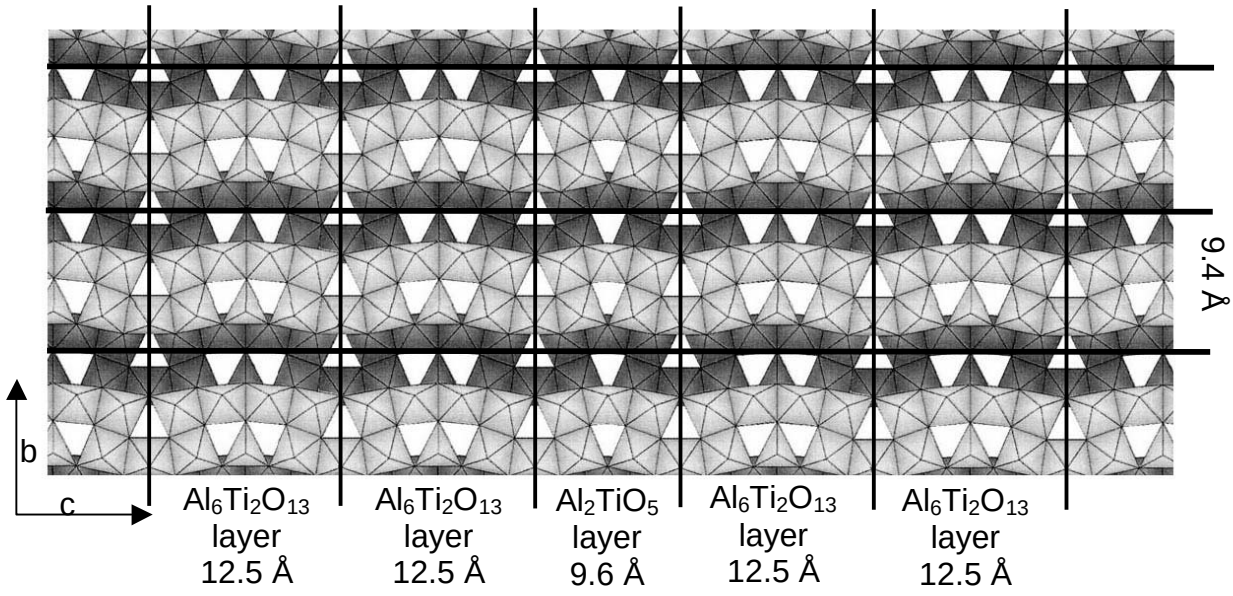

Fig 17: Insertion of a Al_2TiO_5 layer between two $Al_6Ti_2O_{13}$ layers (structure of $Al_6Ti_2O_{13}$ from Norberg et al. [18]).

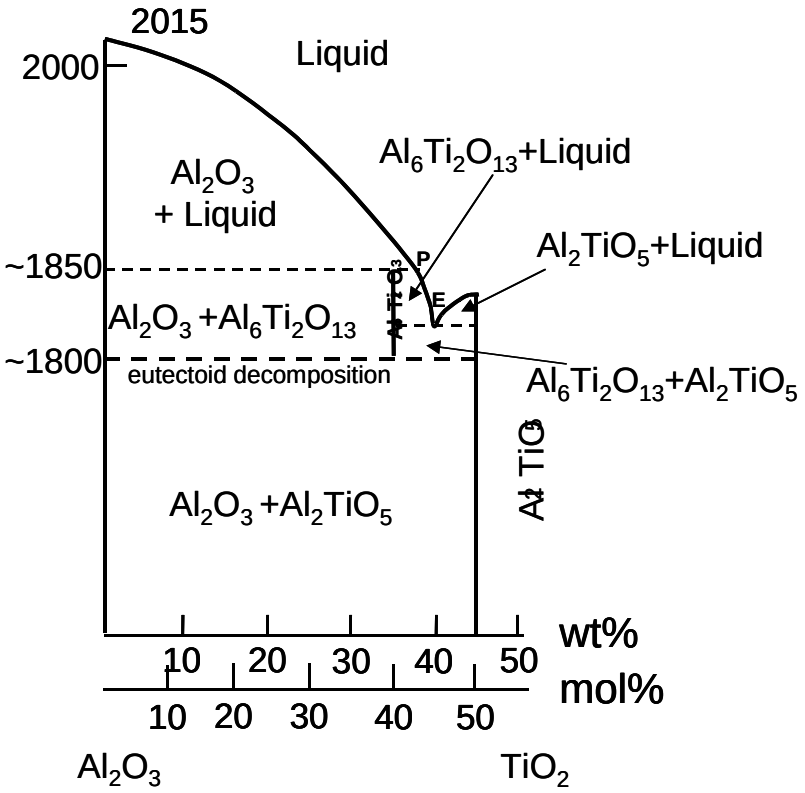

Figure 18: Suggested modification for Al_2O_3-rich part of the Al_2O_3-TiO_2 phase diagram.

Directionally Solidified Boride Eutectics

New initiative entitled Boride Eutectic has been initiated. Project is aims to build multidisciplinary barrier bridging teams to elucidate synthetic chemistry of ultra high temperature eutectic materials development. The boride eutectics LaB_6-MeB_2 (Me = Zr, Hf, Ti, Eu) are currently being developed by Dr. Filipov and Dr. V. Paderno at the Ukrainian Academy of Sciences and modeled by Dr. Kartuzov. The objective is to organize and populate materials property databases, and utilize an iterative feedback routine to constantly improve the design process. The proposed research addresses structural material systems that are highly heterogeneous with a composite media, necessitating a multidisciplinary effort to understand the high temperature strength, creep resistance and emission properties of these in-situ composites on the atomic and microscopic level. As a project director, Dr. Sayir is currently coordinating the management of Boride Eutectic Project and the ongoing research is closely coordinated with Prof. E. Dickey (PSU), Prof. M. Gupta (UV), Dr. S. C. Farmer (NASA GRC), Dr. E. Yadlovsky (HY-Tec Research Corp.), Dr. S. Cytron (US Army ARDEC) and future AFOSR sponsored activities to be determined in the future.

Preliminary data on physical properties of LaB_6-ZrB_2 eutectic have been determined at Southern Research Institute through a subcontract. The specific heat measurements were done to decipher the thermal conductivity values from the heat flux measurements. The specific heat was around 0.64 J/g.m.°C and increased slightly to 0.8 J/g.m.°C leveled of this value after 600 °C as expected from Einstein and Debye's predictions, Fig. 19. The measured thermal conductivity of LaB_6-ZrB_2 eutectic is 115 W/mK at room temperature. . The thermal conductivity decreases monotonically to 75 W/mK at 800 °C, Fig. 20. The linear thermal expansion coefficient

The coefficient of linear expansion is defined as per unit change in length per unit change in temperature, expressed as $\mathrm{CTE}(\alpha) = \left(L - L_0\right)/L_0\left(T - T_0\right)$. CTE is an average coefficient of thermal expansion, which is the one customarily cited in the literature, and different from the differential form (dl/dT) of α. In general, α is a function of temperature and so will refer to α of a particular material at a specific temperature range. The measurement were done at SRI with a custom made dilatometer specifically designed for ultra high temperature region. Dilatometer mostly in forming gas (Argon-5 % hydrogen) environment using 60 ml/min flow rate. Before each run chamber was purged three times either with helium and/or Argon-5 % hydrogen gas to remove residual oxygen. Measurement were successfully done up to 2396 °C and results are shown in Fig. 21. To our knowledge this is the highest temperature range of CTE measurement for this class of material.

The most significant effort was dedicated to measure the uniaxial tensile strength of LaB_6-ZrB_2 eutectic. Drs. V. Flipov and V. Paderno from the Academy of Sciences of Ukraine reported extremely encouraging results for the LaB_6-ZrB_2. To evaluate the strength of LaB_6-ZrB_2 eutectic specimens were tested in uniaxial tension which minimized the off axis loading errors. This approach had it is own disadvantages since it required very specific dog-bone shape geometry. The machining this type of gemotry wit LaB_6-ZrB_2 eutectic was a significant challenge since it's hardness exceeded 25 GPa. The test geometry developed at SRUI was adopted for the tensile strength measurement and data is shown in Figure 22. The micrographs in Fig. 23 shows the fracture surface of LaB_6-ZrB_2 eutectic tested in uniaxial tension. Although results are preliminary, two encouraging results emerge :

1. Tensile strength of LaB_6-ZrB_2 eutectic exceeded 800 MPa. This is a significant strength level for a ultra high temperature material since it was tested in uniaxial loading which is almost always never done in ceramics.

2. Although stress-strain curve does not reveal any graceful failure characteristic of ceramic matrix composites, the fracture surface shows pull-out type of characteristic. Further characterization of these materials are underway to populate the materials data base.

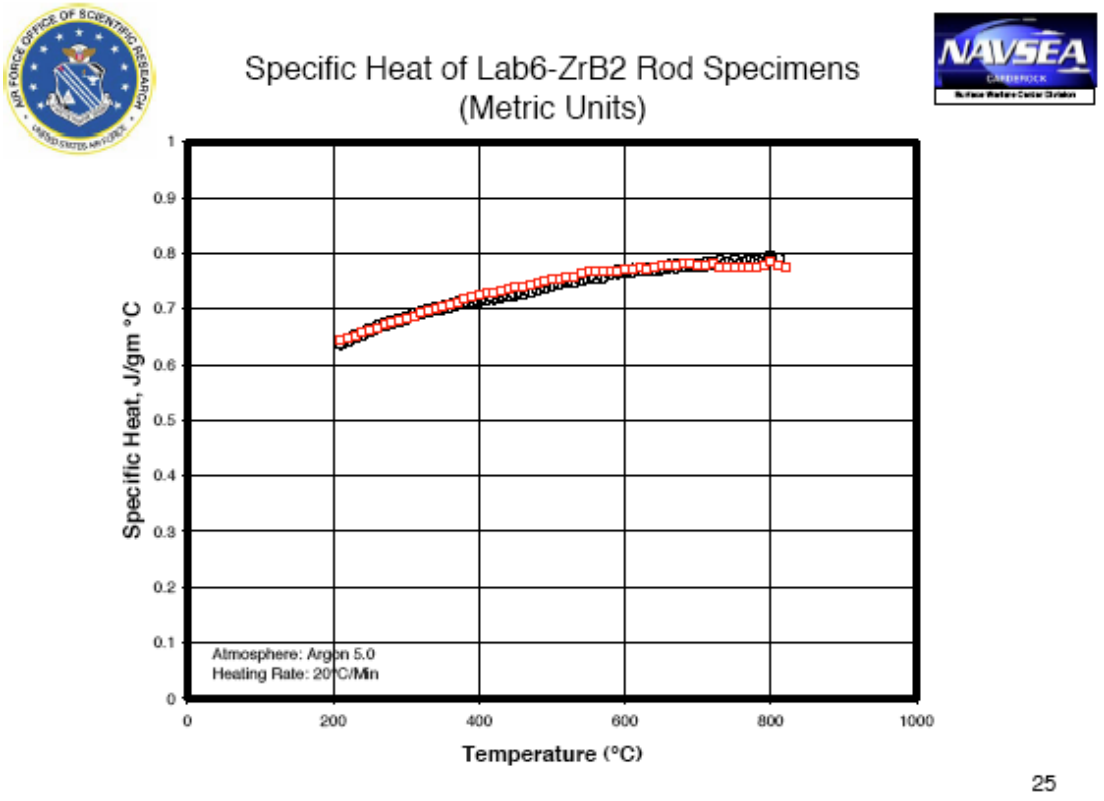

Fig. 19 Specific heat capacity of LaB_6-ZrB_2 eutectic.

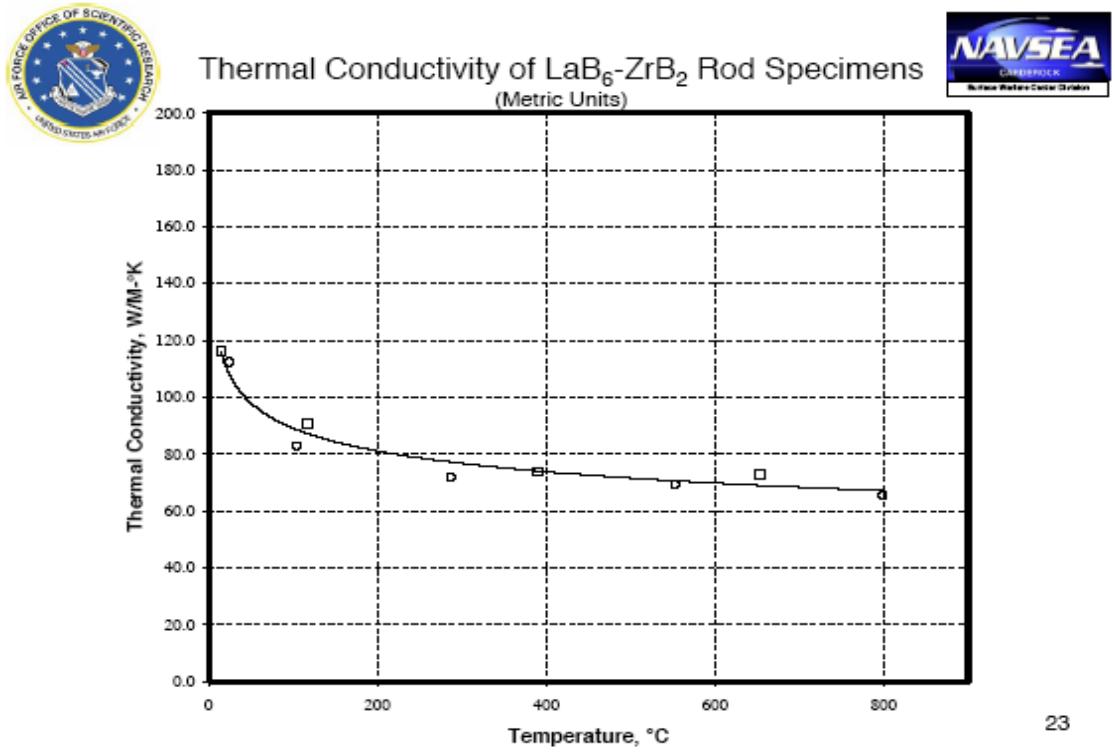

Fig. 20 Thermal conductivity of LaB_6-ZrB_2 eutectic.

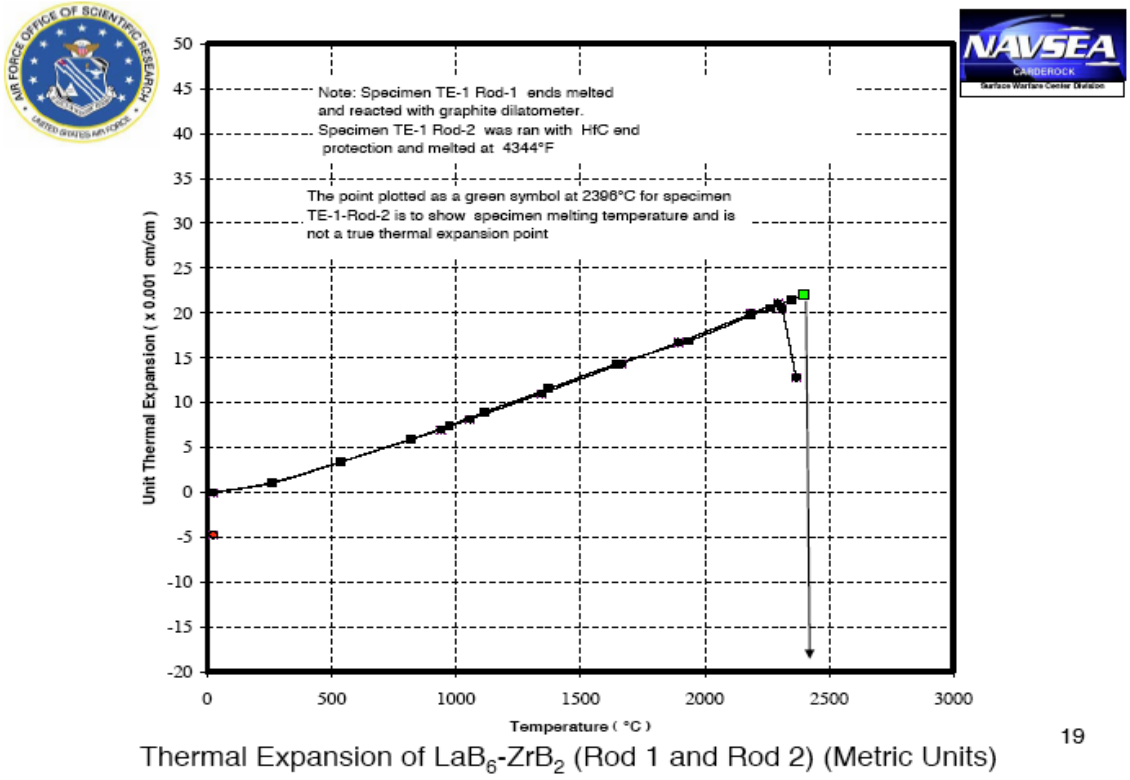

Fig.21 Coefficient of linear thermal expansion coefficient of LaB_6-ZrB_2 eutectic.

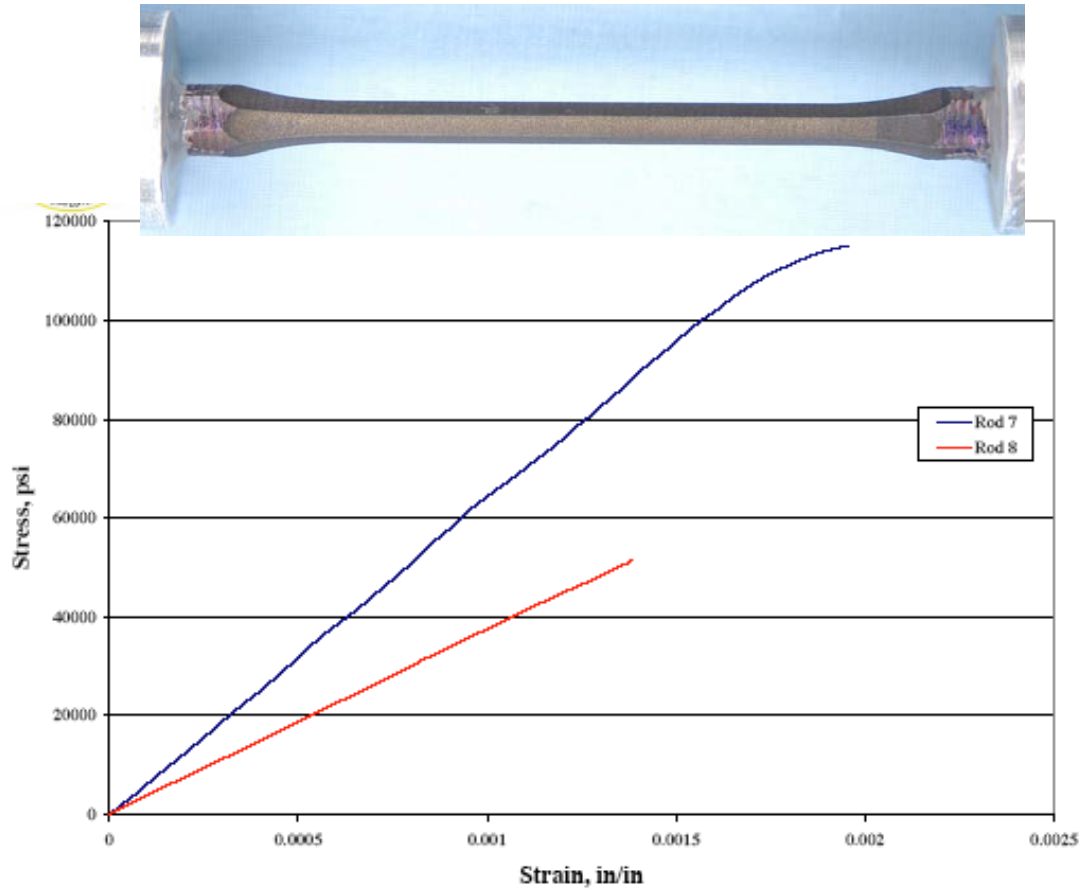

Fig.22 Test geometry and tensile strength of LaB_6-ZrB_2 eutectic.

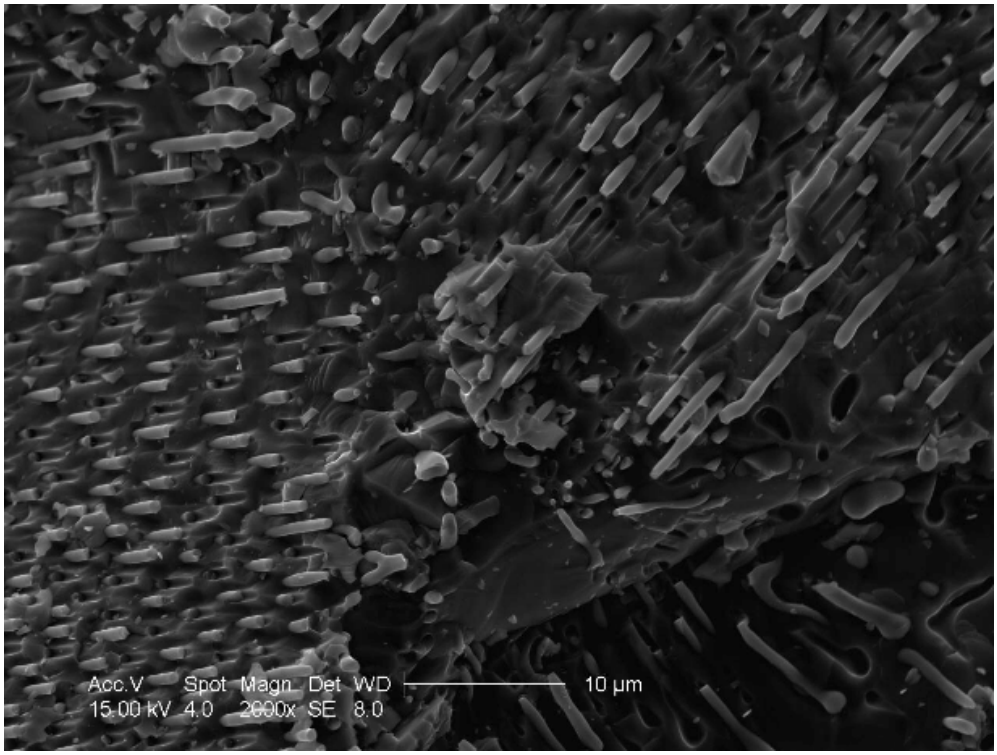

Fig.23 Fracture surface of LaB_6-ZrB_2 eutectic after uniaxial tensile test.

APPENDIX: PUBLICATIONS

REFEREEED JOURNAL PUBLICATIONS

1. J. Yi, A. S. Argon and A. Sayir, "*Internal Stresses and the Creep Resistance of Directionally Solidified Ceramic Eutectics*," Materials Science and Engineering A, 421 (2006) pp 86 - 102.

2. C. Baudin, A. Sayir and M. H. Berger, "*Mechanical Behavior of Directionally Solidified Alumina/Aluminum Titanate Ceramics*," Acta Materialia, Vol. 54 [[14] (2006) pp. 1655 – 1658.

3. P. Berger, H. Khodja, L. Daudin, J-P. Gallien, A. Sayir and M-H. Berger, "*Hydrogen Incorporation into High Temperature Protonic Conductors: Nuclear Microprobe Microanalysis by Means of 1H(p,p)1H Scattering,*" Nuclear Instruments and Methods in Physics Research Section B: Beam Interactions with Materials and Atoms, Vol. 249 [1-2] (2006) pp 527 - 531.

4. J-M. Fernandez, A. R. P. Gomez, J-J. Q. Cancapa, A. R. A. Lopez, J. Llorca, Y. Y. Pastor, S. C. Farmer and A. Sayir, "*High Temperature Plastic Deformation of Er_2O_3 – Doped ZrO_2 Single Crystals*," Acta Materialia, 54 (2006) pp 2195 - 2204.

5. J. Y. Pastor, J. Llorca, P. Poza, J-J. Quispe, J-M. Fernandez, A. R. A. Lopez, A. Sayir, V. M. Orera, "*High Temperature Tensile Strength of Er_2O_3 – Doped ZrO_2 Single Crystals*," Journal of the American Ceramic Society, 89 [7] (2006) pp 2140 - 2146.

6. F. Dynys and A. Sayir, "*Pulsed Laser Deposition of High Temperature Protonic Films*," Solid State Ionics, 177 [26-32] (2006) pp 2333 - 2337.

7. M-H. Berger A. Sayir, F. Dynys, P. Berger, "*Microstructural and Electrical Characterisation of Melt Grown High Temperature Protonic Conductors,*" Solid State Ionics, 177 [26-32] (2006) pp 2339 - 2345.

8. P. Berger, J-P. Gallien, H. Khodja, L. Daudin, M-H. Berger and A. Sayir, "*Nuclear Microprobe Local Hydrogen Measurements in HTPC*," Solid State Ionics, 177 [19-25] (2006) pp 1655 - 1658.

9. M-H Berger, A. Sayir and P. Berger, "*Microstructure, Hydrogen Distribution and Electrical Properties of Melt Grown High Temperature Protonic Conductors*," International Journal of Hydrogen Energy, 31 [8] (2006) pp 1103 - 1111.

10. J. Ramirez-Rico, M. J. Lopez-Robledo, A. R. De Arellano-Lopez, J. Martinez-Fernandez and A. Sayir, "*Fabrication and Microstructure of Directionally Solidified $SrCe_{1-x}Y_xO_{3-\delta}$ (x = 0.1, 0.2) High Temperature Proton Conductors*," Journal of European Ceramic Society, Vol. 26 [16] (2006) pp 3705 - 3710.

11. M. J. Lopez Robledo, J. Ramirez Rico, J. Martinez Fernadez, A. R. de Arellano Lopez and A. Sayir, "*Microestructura y comportamiento plastico de perovsquitas conductoras protonicas de alata temperatura*". Boletin d la Sociedad Espanola de Ceramica y Vidrio, Vol. 44 [5] (2005) pp 347 – 352.

12. F. W. Dynys and A. Sayir, "*Self Assemble Silicide Architectures by Directional Solidification*," Journal of the European Ceramic Society, Vol. 25 [8] (2005) pp 1293 – 1299.

13. J. Yi, A. S. Argon and A. Sayir, "*Creep Resistance of the Directionally Solidified Ceramic Eutectic of $Al_2O_3/ZrO_2(Y_2O_3)$: Experiments and Models,"* Journal of European ceramic Society, Vol. 25 [8] (2005) pp. 1201 -1214

14. A. Sayir, EDITORIAL, Journal of European Ceramic Society, Vol. 25 [8] (2005) pp v.

15. A. Ridruejo, J. Y. Pastor, Javier LLorca, A. Sayir and V. M. Orera, "*Stress Corrosion Cracking of Single-Crystal Tetragonal $ZrO_2(Er_2O_3)$,*" Journal of the American Ceramic Society. 88 [11] (2005) pp 3125 – 3130.

16. K. Miyoshi, S. C. Farmer and A. Sayir, "*Wear Properties of Two-Phase $Al_2O_3/ZrO_2(Y_2O_3)$ Ceramics at Temperatures from 296 to 1073 K*," Tribology International, 38 [11-12] (2005) pp 1 - 13.

17. K. Miyoshi, K. W. Street, R. L. Vander Wal, R. Andrews and A. Sayir, *"Solid Lubrication by Multiwalled Carbon Nanotubes in Air and in Ultrahigh Vacuum*," Tribology Letters, Vol.19 [3] (2005) pp 191 - 2001.

18. Y. B. Paderno, V. B. Filipov, V. N. Paderno and A. Sayir, "*Submicron Size Single Crystal Me(I)(V)B_2 (Me = Ti, Zr, Hf) Fibers*," Journal of the European Ceramics Society., Vol. 25 [8] (2005) pp 1301 - 1305.

19. F. W. Dynys and A. Sayir, "*Self Assemble Silicide Architectures by Directional Solidification*," Journal of the European Ceramics Society, Vol. 25 [8] (2005) pp 1293 - 1299.

20. J. J. Quispe-Cancapa, A. R. de Arellano-Lopez, J. Martinez-Fernandez and A. Sayir, "*Tensile Strength of Directionally Solidified Chromia-Doped Sapphire,*" Journal of the European Ceramics Society, Vol. 25 [8] (2005) pp 1259 - 1268.

21. C. Baudín, A. Sayir and M. H. Berger, "*Failure Mechanisms in Directionally Solidified Alumina-Titania Composites*", Key Engineering Materials, 290 (2005) pp 199 - 202.

PEER REVIEWED CONFERENCE PROCEEDINGS

22. A. Sayir, S. C. Farmer F. Dynys, "*High Temperature Piezoelectric $La_2Ti_2O_7$,"* Ceramic Transactions, Advances in Electronic and Electrochemical Ceramics: Proceedings of the 107th Ann. Mtg. of the Am. Ceram. Soc., Vol. 179 (2006) pp. 57 – 69.

23. M. E.Brito, P. Filip, C. Lewinsohn, A. Sayir, M. Opeka and W. M. Mullins, Editors. Ceramic Engineering and Science Proceedings, "*Developments in advanced Ceramics and Composites*. A collection of papers presented at the 29th International Ceramics and Composites, Vol. 26 [8] (2005) 404p. and PREFACE, Vol. 26 [8] (2005) p ix.

24. A. Sayir, S. C. Farmer F. Dynys, "*Layered structured $La_2Ti_2O_7$ as a High Temperature Piezoelectric,"* High Temperature Electronics, HITEC (2006) TP 15, pp 1 - 8.

25. M. E.Brito, P. Filip, C. Lewinsohn, A. Sayir, M. Opeka and W. M. Mullins, Editors. Ceramic Engineering and Science Proceedings, "Developments in advanced Ceramics and Composites. A collection of papers presented at the 29th International Ceramics and Composites, Vol. 26 [8] (2005) p 404.

26. A. Sayir, M.H. Berger and C. Baudin, "*Microstructural and Mechanical Properties of Directionally Solidified Ceramic in Al_2O_3-Al_2TiO_5 System*," Ceramic Engineering and Science Proc., Vol. 26, [2] (2005) 225 - 233.

27. K. Miyoshi, K. W. Street, R. L. Vander Wal, R. Andrews, D. Jacques, R. L. Vander Wal and A. Sayir, "*Solid Lubrication by Multiwalled Carbon Nanotubes in Air and in Vacuum for Space and Aeronautics Applications*," Proc. of World Tribology Congress III – ASME (2005) pp 321 - 322.